Multiscale estimation of ageing viscoelastic properties of cement-based materials: A combined analytical and numerical approach to estimate the behaviour at early age

Túlio Honório, Benoît Bary, Farid Benboudjema

Multiscale estimation of ageing viscoelastic properties of cement-based materials: a combined analytical and numerical approach to estimate the behaviour at early age

Tulio Honorio corresponding author, *tulio.honorio-de-faria@enpc.fr* , +33 01 64 15 37 50

CEA, DEN, DPC, SECR, Laboratoire d'Etude du Comportement des Bétons et des Argiles, F-91191 Gif-sur-Yvette, France
LMT (ENS Cachan, CNRS, Université Paris Saclay) 94235 Cachan, France
Current adress : Ecole des Ponts Paristech, Laboratoire Navier, 6/8 Avenue Blaise Pascal, 77420 Champs sur Marne, France

Benoit Bary

CEA, DEN, DPC, SECR, Laboratoire d'Etude du Comportement des Bétons et des Argiles, F-91191 Gif-sur-Yvette, France

Farid Benboudjema

LMT (ENS Cachan, CNRS, Université Paris Saclay) 94235 Cachan, France

Abstract:

We propose an investigation combining numerical and analytical tools to estimate the ageing viscoelastic properties of cement-based materials within a multiscale framework. With analytical homogenization the properties at the cement paste and mortar scales are estimated by a combination of Generalized Self-Consistent (GSC) and Mori-Tanaka (MT) schemes. With numerical homogenization the effective properties at the concrete scale are estimated. Numerical homogenization has the advantage of allowing assessing local information and to study more complex geometries. This combined strategy constitutes a promising tool to investigate how different mechanisms leading to ageing at the hydrated products scale, as well as other features of cement-based materials such as the Interfacial Transition Zone (ITZ), affect the viscoelastic behaviour at superior scales. In this context, we study the solidification of non-ageing constituents as the mechanisms leading to the ageing behaviour combined or not with a space-filling process in C-S-H. Relaxation and creep results are presented.

Key words: ageing viscoelasticity; space-filling; homogenization; cement-based materials; early-age.

1. INTRODUCTION

A relevant description of the behaviour of cement-based materials needs to account for the multiscale character of the material [1]. In general, industrial applications demand a good description of macroscopic properties at the relevant scale of application. However, the mechanisms modifying the properties of interest cannot generally be understood at that macroscopic scale. In the case of cement-based materials, these mechanisms occur at different time and space scales. For instance, regarding the specific case of viscoelastic behaviour of such materials, C-S-H behaviour is often reported to be linked to the origin of the viscous effects [2]. In this context, upscaling, or homogenization, techniques are interesting tools to understand and describe properly cement-based materials behaviour.

Using **analytical homogenization**, different properties of cement-based materials can be estimated at early and late ages. The elastic properties of concrete are estimated in e.g. [3–7]; the non-ageing linear viscoelastic properties at late ages can be upscaled by means of analytical techniques in Laplace-Carson space [8]. The *ageing* linear viscoelastic behaviour of concrete was less studied in a multiscale framework. Such constitutive behaviour seems to have been first studied by Maslov [9] to describe concrete behaviour [10]. The *ageing* character is experimentally observed in Portland cement materials due to changes in the microstructure of the material which can be originated, for example, from the pursuit of hydration processes as well as relaxation of hygro-chemically induced self-equilibrated prestress of the microstructure [11,12]. Degradations processes (e.g. leaching), which can be coupled with the viscoelastic behaviour of the material itself, can be also a source of the ageing behaviour. In the following, we focus on the early-age in which the hydration processes play a major role in the ageing aspect.

In this regard, Scheiner et al. [13] proposed an upscaling strategy using Mori-Tanaka (MT) and Self-Consistent schemes in Laplace-Carson space. Homogenization is applied at cement paste, mortar and concrete scales. The creep and relaxation tensors were obtained by numerical inversion of Laplace transforms. Then, the resulting ageing behaviour of the material was obtained by integration over the changes in the volume fraction of the constituents in time. The evolutions of the volume fraction are described by JMAK equations combined with a simplified description of the phases potentially present in the hydration processes. Another recent proposition in the direction of estimating the ageing linear viscoelastic behaviour of cement-based materials is made by Sanahuja [14]. Even if the full description of the scales of interest in cement-based material (from C-S-H up to concrete) is still not made, the author proposes a derivation of some classical homogenization schemes using formalism based on Volterra integral operator. This formalism allows establishing a correspondence between elasticity and ageing linear viscoelasticity [15,16]. Dilute, MT, Self-Consistent [14] and Generalized Self-Consistent (GSC) schemes [17] can be derived in an ageing linear viscoelastic framework in this way.

Correspondingly, using **numerical homogenization**, the elastic and non-ageing viscoelastic properties of concrete were estimated by different authors (see e.g. [18–23]) in studies of the long-term behaviour of concrete. Early-age investigations require a specific approach to deal with the evolution of the microstructure at the cement paste level. In this respect, the works involving the platforms *µic* [24,25], *CEMHYD* [26] and *Hymostruc* [27] are potentially leading-edge by allowing coupling hydration microstructure-based models with FEM (or other numerical methods) simulations to determine the effective properties of cement-based materials at early age. Once again, the ageing linear viscoelastic behaviour at early age was less studied. In this respect, for 2D mesostructures we highlight the works of Briffaut et al. [28]. Do et al. [25] estimated the ageing viscoelastic behaviour by means of FEM simulations with outputs of *µic* platform [24]; a scenario in which the space-filling intervenes in the C-S-H behaviour was studied by the author.

In this paper, we propose an investigation combining numerical and analytical tools to estimate the ageing viscoelastic properties of cement-based materials within a multiscale framework. With analytical homogenization the properties at the cement paste and mortar scale are estimated by a combination of GSC and MT schemes. With numerical homogenization the effective properties at the concrete scale are estimated. Numerical homogenization has the advantage of allowing to assess local information as well as to study more complex geometries. This combined strategy constitutes a promising tool to investigate how different mechanisms leading to ageing at the hydrated products scale, as well as other features of cement-based materials such as the Interfacial Transition Zone (ITZ), affect the viscoelastic behaviour at superior scales. Such strategy was previously used by the authors to estimate elastic properties [29] and ageing viscoelastic properties [30] of cement based-materials. Here, a more comprehensive and detailed analysis is provided regarding the latter case.

No effects of drying and temperature on the viscoelastic behaviour are considered in this paper. In other words, we are only dealing with *basic* creep and relaxation phenomena. Also, the discussion is focused on the early-age behaviour, so the mechanisms acting in the long-term behaviour are not accounted for. In the estimations presented in this work, we assume that a percolated structure exists at the different levels. At very early-age this assumption is not true. This limits the scope of applicability of this work to periods after the percolation threshold.

2. MULTISCALE STRATEGY

As mentioned in the Introduction, analytical homogenization is used to estimate the properties at the cement paste and mortar scale (Figure 1). A two-coated sphere morphology is used to represent the cement paste and mortar microstructures [29,30], as proposed previously by e.g. [31,32].

Regarding the cement paste, the hydrating particle is embedded in a high density (HD) products layer which is, in turn, embedded in a low density (LD) products layer. Following Bary and Béjaoui [31], we assume that the scale of these two subproblems is not the same since the typical size

of the inclusions ranges from < 1 μm up to several tens of micrometre for massive crystals, whereas the characteristic length scale of C–S–H is 1 to 100 nm [33].

Regarding the mortar, the sand particle is embedded in an ITZ layer which is, in turn, embedded in a cement paste layer. The GSC scheme is used to obtain the homogenized properties of the cement paste and mortar. MT scheme is used to estimate the properties within each coat. The formulations of the schemes in ageing linear viscoelasticity are presented in Section 3.

Numerical homogenization is used to estimate the properties at the concrete scale. A specific procedure associated with the Finite Elements code Cast3M (http://www-cast3m.cea.fr/) to generate and compute 3D microstructures is used [34,35]. Local information regarding the stresses and strains repartition in the heterogeneities and in definite regions of the matrix are assessed. This is an advantage compared to analytical schemes that generally provide accurate estimations only on per phase averaged fields. With the local information, the zones in which stresses are localized can be more precisely identified. Previous results showed that a considerable dispersion of the averaged stresses within the inclusions and matrix subvolumes is observed [36].

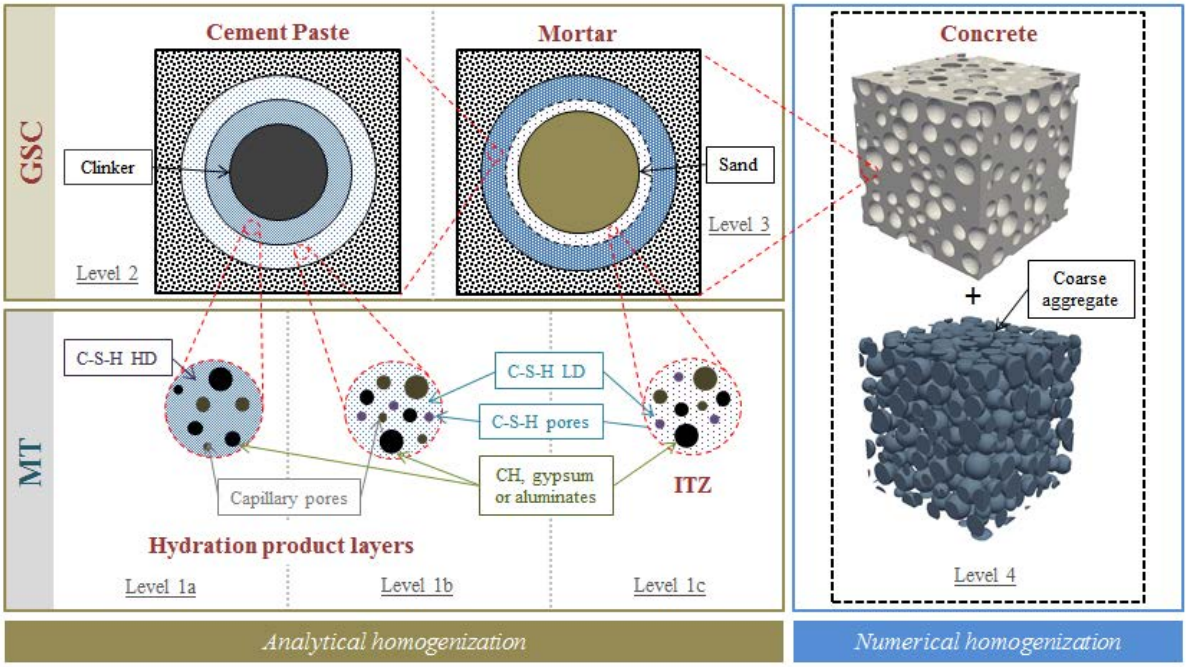

Figure 1 Multiscale strategy with combined analytical and numerical homogenization

3. ANALYTICAL HOMOGENIZATION: MT AND GSC ESTIMATIONS

As previously mentioned, the derivation of the analytical homogenization schemes, needed in the proposed multiscale strategy, is performed in a specific ring in which Volterra correspondence principle (with respect to elasticity) holds [15,16]. With this correspondence principle the ageing linear viscoelastic behaviour can be upscaled.

In a set F of functions f, we define a ring $(F;+,\circ)$ in which the binary operator satisfies the conditions defining a division ring (or skew field), i.e. all nonzero elements have a multiplicative inverse but the multiplication is not necessarily commutative. The multiplication operator "$\circ$" is Volterra [37] integral operator defined as:

$$(f \circ g)(t,t_0) \equiv \int_{t'=-\infty}^{t} f(t,t')\, d_{t'} g(t',t_0) \tag{1}$$

Similarly, we can define a ring for a set of matrices **F** and the Volterra matrix inner product $\left(\mathbf{F};+,\overset{\circ}{\cdot\cdot}\right)$ and for a set of tensors $\mathbb{F}$ and the Volterra tensor product $\left(\mathbb{F};+,\overset{\circ}{\vdots}\right)$. For these division rings, the identity elements are $H_{t'}(t)\,\mathbf{I}$ and $H_{t'}(t)\,\mathbb{I}$, where **I** and $\mathbb{I}$ are the matrix and fourth order identity tensors, respectively.

Within this ring, the stress-strain relationships in ageing linear viscoelasticity, within a volume **Ω,** can be written as [15]:

$$\boldsymbol{\varepsilon}(\mathbf{x},t) = \mathbb{S}(\mathbf{x},t,.) \overset{\circ}{\vdots} \boldsymbol{\sigma}(\mathbf{x},.), \qquad \forall \mathbf{x} \in \boldsymbol{\Omega} \tag{2}$$

$$\boldsymbol{\sigma}(\mathbf{x},\boldsymbol{t}) = \mathbb{R}(\mathbf{x},\boldsymbol{t},.) \overset{\circ}{\vdots} \boldsymbol{\varepsilon}(\mathbf{x},.), \qquad \forall \mathbf{x} \in \boldsymbol{\Omega} \tag{3}$$

where the relaxation and compliance tensors, $\mathbb{R}$ and $\mathbb{S}$, respectively, can be obtained from each other by the inversion with respect to the operator "$\overset{\circ}{\vdots}$":

$$\mathbb{S} \overset{\circ}{\vdots} \mathbb{R} = \mathbb{R} \overset{\circ}{\vdots} \mathbb{S} = H_{t'}\, \mathbb{I} \tag{4}$$

Note that, since the multiplication is not necessarily commutative, the order between the factors is important in the derivation of the schemes using this formalism.

The MT and GSC estimations in ageing linear viscoelasticity, which are used in the analytical part of this paper, are briefly presented in the following.

3.1 MT ESTIMATIONS

Mori and Tanaka [38] proposed estimations in elasticity of the effective properties of composites with a matrix-inclusions morphology. In their derivation, based on Eshelby solution in elasticity for an inclusion in an infinite medium, the matrix is the reference medium and the phase interaction is taken into account in a collective way [38].

In the ageing linear viscoelastic framework, for spherical inclusions, Mori-Tanaka estimations of the bulk and shear relaxation functions for a *N*-phases composite are given, respectively, by [15]:

$$k_{MT} = \left(\sum_{i=0}^{N} f_i^v k_i \circ {}^{k}A_i^0\right) \circ \left(\sum_{i=0}^{N} f_i^v \, {}^{k}A_i^0\right)^{-1} \tag{5}$$

$$\mu_{MT} = \left(\sum_{i=0}^{N} f_i^v k_i \circ {}^{\mu}A_i^0\right) \circ \left(\sum_{i=0}^{N} f_i^v \, {}^{\mu}A_i^0\right)^{-1} \tag{6}$$

where f_i^v is the volume fraction of the phase (i) (with $i = 0$ corresponding to the matrix and $i > 0$ corresponding to the inclusions). The localization tensor within the spherical inclusions was decomposed in a hydrostatic and deviatoric parts given, respectively, by [15]:

$${}^{k}A_i^0 = (3k_i + 4\mu_0)^{-1} \circ (3k_0 + 4\mu_0) \tag{7}$$

$${}^{\mu}A_i^0 = H_{t'} + 2(2H_{t'} + 3\Xi) \circ [2\mu_i \circ (2H_{t'} + 3\Xi) + 2\mu_0 \circ (6H_{t'} - \Xi)]^{-1} \circ (\mu_0 - \mu_i) \tag{8}$$

with ${}^{j}A_0^0 = {}^{k}A_0^0 = H_{t'}\,\mathbf{I}$ and $\Xi = \frac{2}{3}(k_0 + \mu_0)^{-1} \circ \mu_0$. As expected, these estimations of k_{MT} and μ_{MT} are a generalization of the results in elasticity and non-ageing viscoelasticity.

3.2 GSC ESTIMATIONS

Generalized Self-Consistent estimations are based on a morphology with a *n*-coated isotropic spherical inclusion embedded in an infinite matrix, which is subjected to a uniform stress or strain applied at infinity [39]. Application of such scheme in the estimation of effective properties of cement-based materials [5,29,31,32] is quite convenient. For example, at the cement paste scale, layers with high and low density products are observed coating the cement particle. Also, at the mortar scale, an interface transition zone (ITZ) coats the sand and coarse aggregates particles.

The GSC estimation of the bulk relaxation function in ageing linear viscoelasticity for a n-phase composite is given by [17]:

$$k_{\mathrm{GSC}}^{(n)} = k_{n+1} = \left[3{R_n}^3 k_n \circ Q_{11}^{(n-1)} - 4\mu_n \circ Q_{21}^{(n-1)}\right] \circ \left[3{R_n}^3 Q_{11}^{(n-1)} + 3Q_{21}^{(n-1)}\right]^{-1} \tag{9}$$

with matrix $\mathbf{Q}^{(i)}$ being the product in the sense of Volterra operator matrix product $\overset{\circ}{\ast}$ of matrix $\mathbf{N}^{(i)}$:

$$\mathbf{Q}^{(i)} = \overbrace{\prod_{j=1}^{i} \mathbf{N}^{(j)}}^{\overset{\circ}{\ast}} \tag{10}$$

$$\mathbf{N}^{(i)} = [4\mu_{i+1} + 3k_{i+1}]^{-1} \circ \begin{bmatrix} 4\mu_{i+1} + 3k_i & \frac{4}{{R_i}^3}(\mu_{i+1} - \mu_i) \\ 3{R_i}^3(k_{i+1} - k_i) & 3k_{i+1} - 4\mu_i \end{bmatrix} \tag{11}$$

The estimation of shear relaxation function is lengthier and is not shown here for conciseness. See Honorio et al. [17] for details about the derivation of GSC estimation in ageing linear viscoelasticity.

4. C-S-H BEHAVIOUR

The origin of the viscoelastic behaviour of cement-based materials is often reported to come from the C-S-H behaviour [2], and different mechanisms are proposed in the literature to explain it [40–43]. Moreover, at early-age, the viscoelastic behaviour becomes ageing.

The identification of C-S-H viscoelastic parameters is generally done by means of indirect approaches. Sanahuja and Dormieux [44] propose a micromechanical modelling of C-S-H based on the relative sliding of the sheets with nanogranular C-S-H grains. Spheroidal grains with isotropic orientation are considered. With this representation, the resulting non-ageing viscoelastic behaviour of the elementary particle is obtained by means of the correspondence principle in Laplace-Carson domain. The model accounts for one single level to represent the C-S-H structure. Their results are function of the porosity φ_{gel} found in-between the grains. Smilauer and Bazant [45] estimated the C-S-H viscoelastic properties by means of a microstructural inverse analysis from creep data of cement paste or concrete.

Vandamme and Ulm [43,46] studied the viscoelastic behaviour of C-S-H from statistical analysis of nanoindentation tests. They obtained the following formula for uniaxial creep compliance which can be written as a function of the contact creep C_v:

$$J_{un}(t,t_0) = \frac{1}{E} + \frac{1}{C_v(1+v^2)} \ln\left[1 + \frac{t-t_0}{\tau}\right] \tag{12}$$

where τ is a characteristic time. The mean value of τ obtained by [43] is 1.66 s, which characterizes a quite fast progress of viscous processes with a pronounced evolution within the first 3 days after what an asymptotic regime is reached. The contact creep compliance was obtained by fitting nanoindentation data [43]:

$$C_v(\eta_p) = 1588.9\langle \eta_p - 0.5 \rangle_+^{1.597} \tag{13}$$

where η_p is the packing density of C-S-H and $\langle . \rangle_+$ is the positive part operator. Note that with this equation the packing density is characterized by a percolation threshold of 50 % of solid inclusions. In the following, this behaviour is retained for C-S-H. Regarding the ageing aspect, two scenarios are studied:

1. Two constant packing densities are attributed respectively to C-S-H to represent the behaviour of High Density (HD) and Low Density (LD) C-S-H. The resulting intrinsic behaviour is non-ageing, this aspect being accounted for by adequate precipitation mechanisms (see [40]).

2. The packing density evolves according to a space-filling kinetics. The resulting behaviour is intrinsically ageing.

These two scenarios are developed and the corresponding C-S-H behaviours are expressed in the two following subsections.

4.1 C-S-H VISCOELASTIC BEHAVIOUR WITHOUT SPACE-FILLING: NON AGEING

The behaviour of LD and HD C-S-H can be determined by defining a given packing density for each type. The packing densities 0.66 and 0.77 were retained for LD and HD C-S-H, respectively. The first value corresponds to the one identified by [43] for the LD C-S-H. The second one corresponds to an intermediary value between the HD and the UHD (Ultra-High Density) C-S-H, as identified by Vandamme and Ulm [43,46], whose mean packing density values are 0.75 and 0.83, respectively.

Assuming a constant Poisson ratio $v^{C-S-H} = 0.24$ the behaviour law of both C-S-H may be expressed by [16]:

$$\boldsymbol{\varepsilon}(t) = (1 + v^{C-S-H})\, \mathbf{J}^{\boldsymbol{C-S-H}}(t, t_0) \mathbin{\mathring{\vdots}} \boldsymbol{\sigma} - v^{C-S-H}\, \mathbf{J}^{\boldsymbol{C-S-H}}(t, t_0) \mathbin{\mathring{\vdots}} (\mathrm{tr}\, \boldsymbol{\sigma})\mathbf{I} \qquad (14)$$

From that it is possible to determine the volumetric and deviatoric parts of the compliance tensor, J_k^{C-S-H} and J_μ^{C-S-H}, respectively, as shown in Figure 2 for the HD and LD C-S-H whose behaviour is non-ageing. Based on the solidification theory as proposed by Bazant [40] which shows that a viscoelastic ageing behaviour can be obtained from non-ageing phases in the presence of precipitation processes, the ageing character of both C-S-H is then obtained by applying appropriate formation kinetics to these phases. This will be detailed in the following.

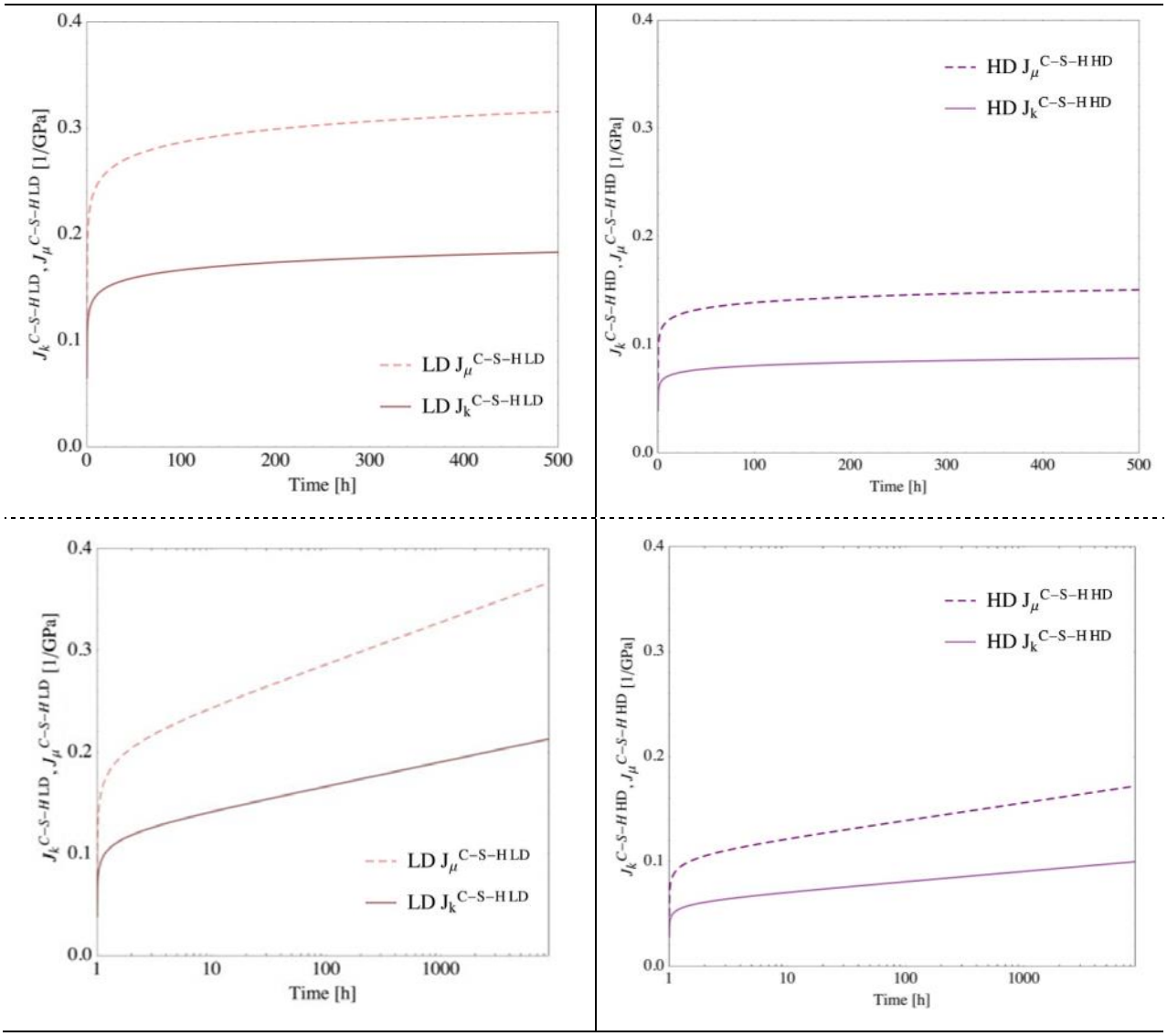

Figure 2 C-S-H HD and LD deviatoric and volumetric components of compliance tensor: non-ageing behaviour at short (top) and long (bottom) term, no space filling accounted for.

4.2 C-S-H VISCOELASTIC BEHAVIOUR WITH SPACE-FILLING: INTRINSICALLY AGEING

Another strategy is to account for a space filling process (or compaction [47], or densification [48]) within C-S-H to describe its ageing nature, which results in an intrinsically ageing behaviour. To describe such space-filling process we propose to use a version of Bishnoi and Scrivener [48] space-filling kinetics:

$$\eta_p(t) = \frac{\rho(t)}{\rho_{max}^{pack}} = 1 - \frac{(\rho_{max} - \rho_{min})}{\rho_{max}} \exp\left[\frac{-k_{DEN}}{\rho_{max} - \rho_{min}}(t)\right] \quad (15)$$

with ρ_{max}^{pack} = 2.2 g/cm^3 and ρ_{min}= 0.2 g/cm^3; k_{DEN}= 0.02 g/cm^3/h [49]. For the HD C-S-H, $\rho_{max} = \rho_{max}^{pack}$, so the asymptotic value of η_p is 0.77 as in the previous section. For the LD C-S-H, ρ_{max} = 1.88, so the asymptotic value of η_p is 0.66, as in the previous section. Figure 3 shows the resulting evolutions of the packing density. Note that at the beginning of the hydration, the evolution

of the packing density is quite close for both types of C-S-H; this is in agreement with the experimental observation in which HD product is only distinguishable at later times [50]. Note that Do [25] similarly proposed a space-filling kinetics to define an intrinsically ageing behaviour to C-S-H. Further studies in the direction of the determination of the kinetics of space-filling can be envisioned.

The resulting behaviour in terms of volumetric and deviatoric components of compliance tensor is shown in Figure 4 and Figure 5 for different loading ages t_0. These figures clearly show the effects of ageing on C-S-H creep functions. Note that the earlier the loading time, the higher is the slope of logarithmic creep in both volumetric and deviatoric cases. For loading times after about 150 h the ageing character almost vanishes.

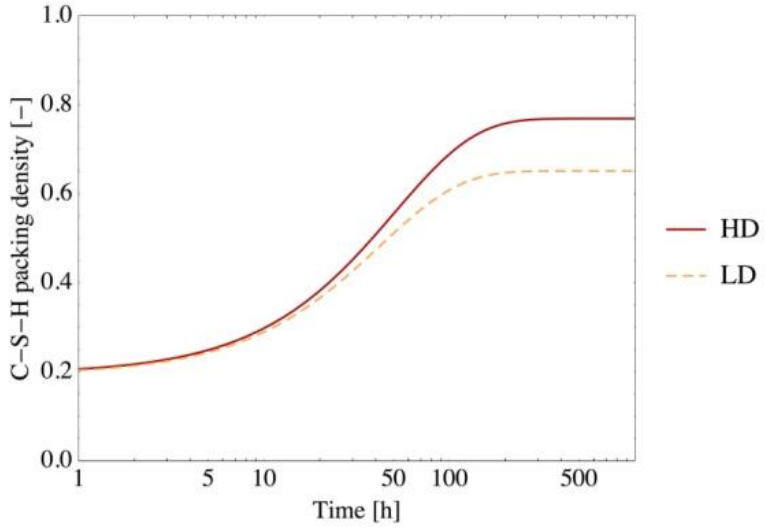

Figure 3 C-S-H packing density evolution according to Eq. (15)

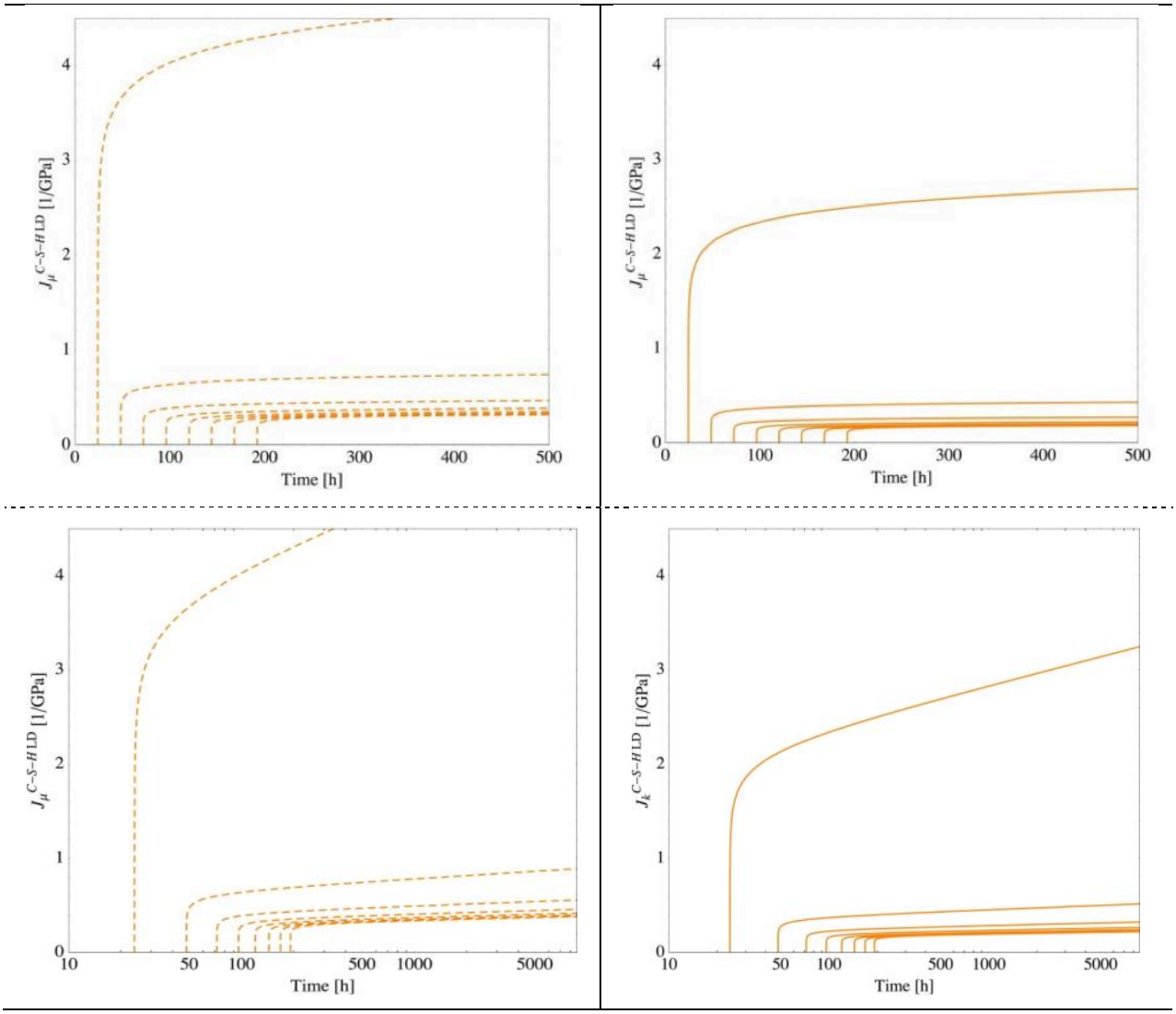

Figure 4 C-S-H LD deviatoric and volumetric components of compliance tensor for different loading ages: intrinsically ageing short (top) and long (bottom) term behaviour accounting for space filling process.

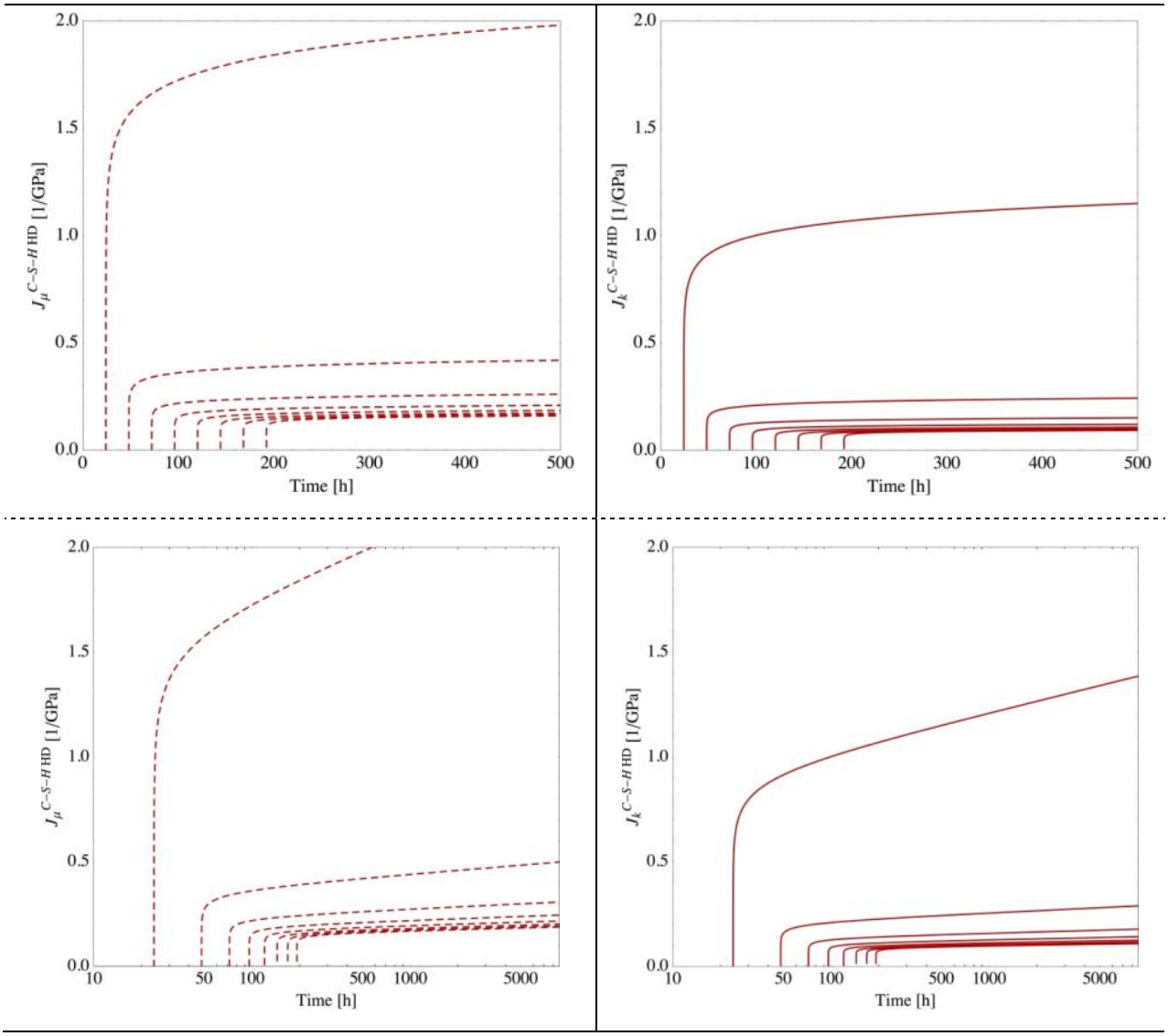

Figure 5 C-S-H HD deviatoric and volumetric components of compliance tensor for different loading ages: intrinsically ageing short (top) and long (bottom) term behaviour accounting for space filling process.

5. CEMENT PASTE SCALE

At the cement paste scale, the evolutions of the volume fractions of the cement minerals and hydration products have to be accounted for. Following the microstructure representation in Figure1, two levels are identified:

- Level 1a and 1b of the inner products and outer products in which C-S-H HD and C-S-H LD, respectively, function as a matrix in which the other hydration products and capillary pores are embedded.
- Level 2 in which the previous layers of inner and outer products are taken into account in composite inclusions morphology.

In this representation an evolution of the volume fraction occurs at both levels. At level 1, the volume fraction of non-bonded water decreases with its consumption by hydration reactions and the volume fraction of the forming products take the left place. At level 2, the dissolving clinker particle leaves place to the growing of inner product layer.

The analytical upscaling tools developed in [15,17] can be applied iteratively to represent these volume changes due to dissolution and precipitation.

5.1 EVOLUTION OF PRODUCTS AND REACTANTS IN HYDRATION PROCESS

Based on Honorio et al. [49], a simplified (semi)-analytical kinetics model of hydration is employed together with Tennis and Jennings [42] hydration balance to obtain the evolution of the volume fraction of hydration products and reactants. The kinetics of hydration is based on boundary nucleation and space-filling growth with a fixed confined zone imposed for early hydration and a diffusion-controlled kinetics for late hydration for which the Particle Size Distribution (PSD) of cement particles is explicitly accounted for [49]. The reaction zone is defined by a combination of an exponential box and a fixed limiting parameter.

The same cement studied in [49] (type CEM I 42.4 N-SR3, i.e. with a low C_3A content) is studied here. The composition of this cement is shown in Table 1 and the PSD in Figure 6. The w/c ratio is 0.50. The contribution of each clinker mineral on the overall degree of hydration is shown in Figure 7. The repartition of the products in High Density and Low Density layers is made proportionally to the volume of C-S-H in the layer (Figure 8). A part of the products is reserved to the ITZ, as will be discussed in Section 6.1.

Table 1 Normative cement composition [49]

Mineral	Initial mass fraction [%]
$\mathbf{C_3S}$	64.0
$\mathbf{C_2S}$	23.1
$\mathbf{C_3A}$	1.5
$\mathbf{C_4AF}$	2.0
$\mathbf{C\bar{S}H_2}$	2.0
Others	7.35

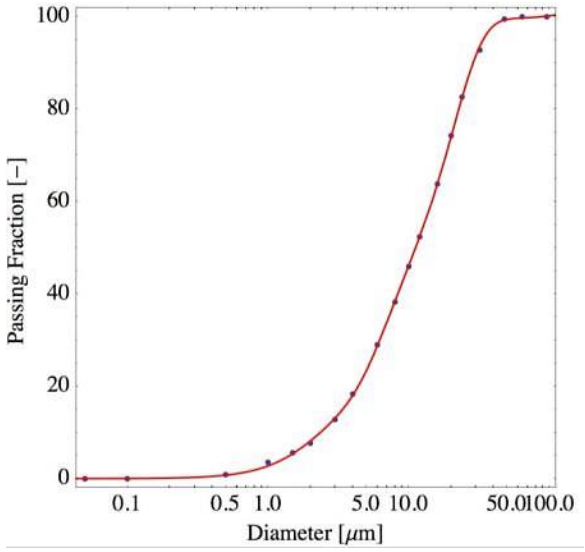

Figure 6 Passing PSD of cement: fitted (full lines) and experimental (dots) data [49]

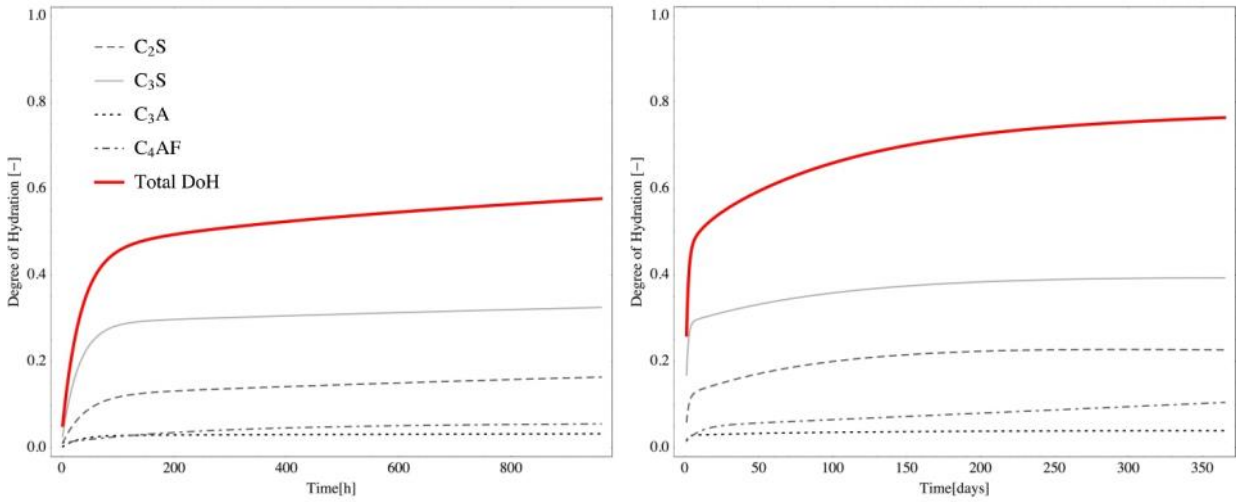

Figure 7 Contribution of each clinker mineral on the overall degree of hydration (the curves corresponding to the clinker mineral are the degree of hydration of the mineral weighted by its content at a given time): early (left) and late (right) behaviours

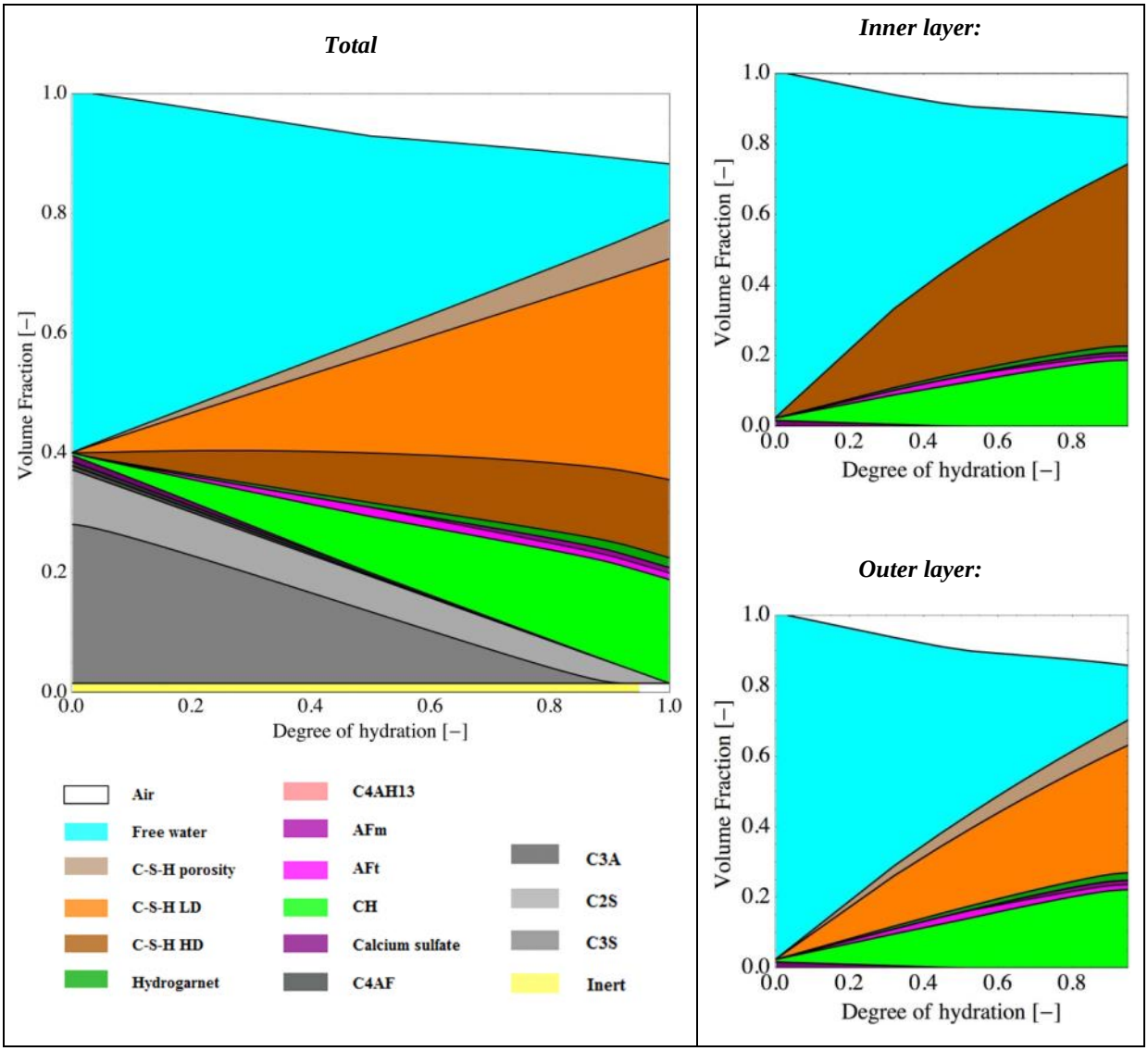

Figure 8 Repartition of the products: Inner and Outer products. The ITZ is shown in Figure 17.

5.2 DISSOLUTION/PRECIPITATION AND SOLIDIFICATION MECHANISMS

As previously mentioned, Bazant [51] showed that an ageing effective behaviour can be observed in materials in which one of the constituents shows a change in its volume fraction in time, as occurs for example in a solidification process. This effect is observed even if the basic constituents are non-ageing themselves [40]. This so-called solidification theory can be extended to a general form in which dissolution and precipitation of multiphasic systems occur in more complex configurations (Figure 9 and Figure 10, for instance). Sanahuja [14] proposed a tensorial extension of this theory. The relaxation tensor for a given phase solidifying at time t_i^s is identified by:

$$\mathbb{R}_i(t, t_0) = \mathbb{R}_s(t - t_0)\,\mathrm{H}(t_0 - t_i^s) \tag{16}$$

where $\mathbb{R}_s(t - t_0)$ is the relaxation tensor of the solidified material and t_0 is the age of loading.

The solidification can occur following different processes. Generally the assumption of dissolution followed instantaneously by precipitation is adopted. Sanahuja [14] studied cases in which the precipitation can occur in two different ways: inwards pores or by occupying entirely and instantaneously some class of pores. The changes in the volume fraction of phases are taken into account with analytical homogenization by applying iteratively the upscaling schemes. This strategy involves a discretization of the ageing function in n steps. Here, as in [14], the solidification times are chosen so that the same volume fraction of solid f_{age}^{∞}/n precipitates at each t_i^s. Correspondingly, we have [14]:

$$f_{age}(t_i^s) = \left(i - \frac{1}{2}\right) \frac{f_{age}^{\infty}}{n} \tag{17}$$

with f_{age}^{∞} being the final value of the volume fraction of the phase solidifying. The estimation of the effective properties then is made by determining the properties of a fictitious n-phases composite. Sanahuja [14] showed that the precipitation mechanism and the kinetics of the ageing process affect directly the effective ageing viscoelastic response.

Here, an evolution function is attributed to each phase present in the paste according to the hydration kinetics model of cement presented in section 5.1. The hydration products other than C-S-H are assumed to behave purely elastically; the corresponding elastic properties of the different phases are shown in Table 2.

According to the representation of the microstructure presented in section 2, two levels in which the solidification process occurs can be identified. At the level of the hydrates layers (1a, 1b and 1c), we assume that the pores are completely filled in according to the evolution laws corresponding to each hydrate (Figure 9). Next, at the cement paste level, with the GSC scheme we assume that the HD layer fills instantaneously the space left by the clinker, as shown in Figure 10.

Table 2 Elastic properties of the different phases

	Clinker	**C-S-H**		**CH**	**AFt**	**AFm**	**$C_3(A,F)H_6$**	**C_4AH_{13}**	**Gypsum**	**Sand**
		LD	**HD**							
E [GPa]	140	21.7	29.4	38	22.4	42.3	22.4	25	45.7	74.5
ν	0.3	0.24	0.24	0.305	0.25	0.324	0.25	0.25	0.33	0.2
Ref.	**	^^	^^	§§	%%	%%	°°	°°	°°	##

**[52]; ^^[3]; §§[53]; %%[54];°°[55]; ##[56]

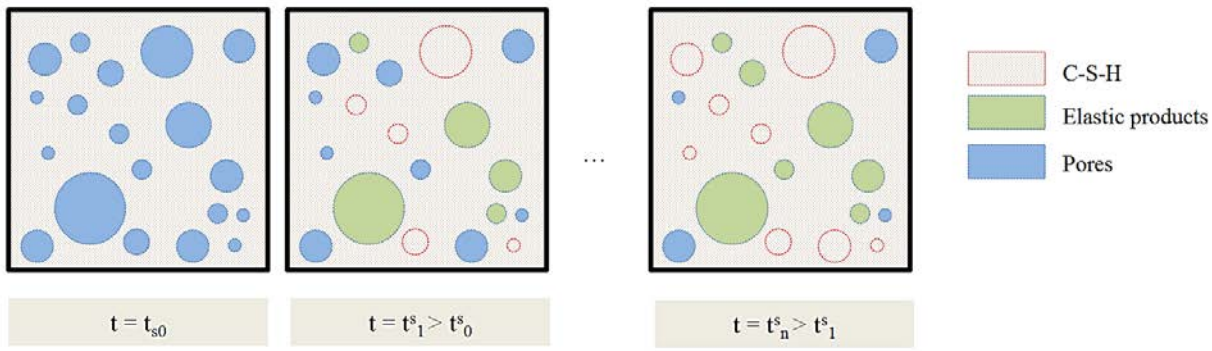

Figure 9 Schematic representation of the solidification process adopted at the hydrates layers (Levels 1a, 1b and 1c)

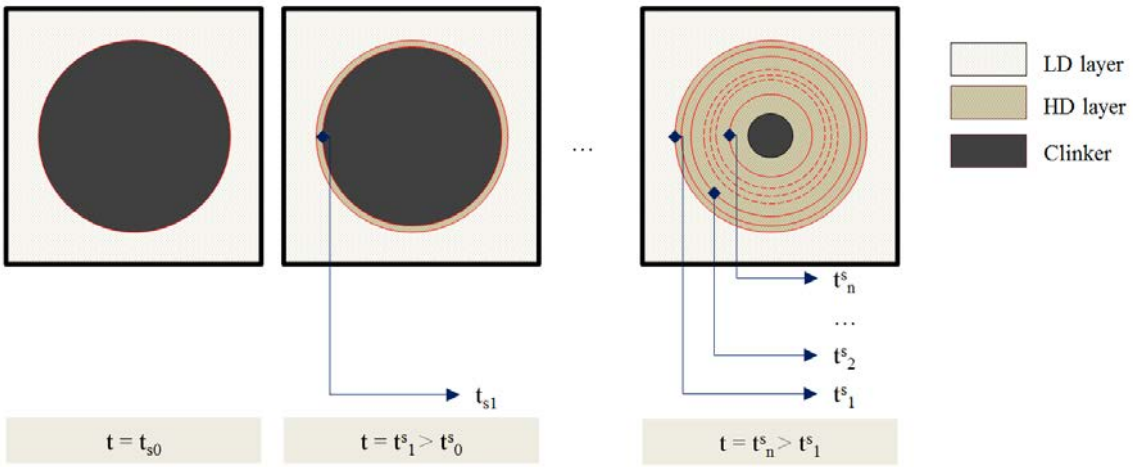

Figure 10 Schematic representation of the solidification process adopted at the cement paste level (Level 2)

5.3 EFFECTIVE PROPERTIES AT THE CEMENT PASTE SCALE

The effective bulk and shear relaxation functions of the inner and outer layers (Level 1a and 1b) are shown in Figure 11 for the behaviours with and without space filling. Note that, because of the solidification process, the effective behaviour is ageing for both cases. A similar response at late ages (after 400 h) is observed in both cases. As expected, most part of the evolution in the elastic response occurs within the first 200 h, in agreement with the evolution of C-S-H volume fraction as obtained by the hydration model. In Figure 11, this ageing function is discretised in 50 parts ($n_{sol} = 50$), corresponding to times in which a same volume of C-S-H precipitates.

The evolution of properties with the behaviour in which space filling is accounted for is slower compared to the other case. The influence of the ageing function discretization is presented in Figure 12 for the case with space filling. Note that the elastic response for each loading age depends on this discretization. Increasing the discretization, a smoother evolution of this elastic response is observed. Correspondingly, stronger discontinuities in the evolution are obtained for coarser discretizations of

the ageing function. Since the curves are enveloped by the ageing elastic response, the relaxation moduli are then underestimated with coarser discretizations of the ageing function. The same behaviour is as expected observed with the case in which no space filling is considered.

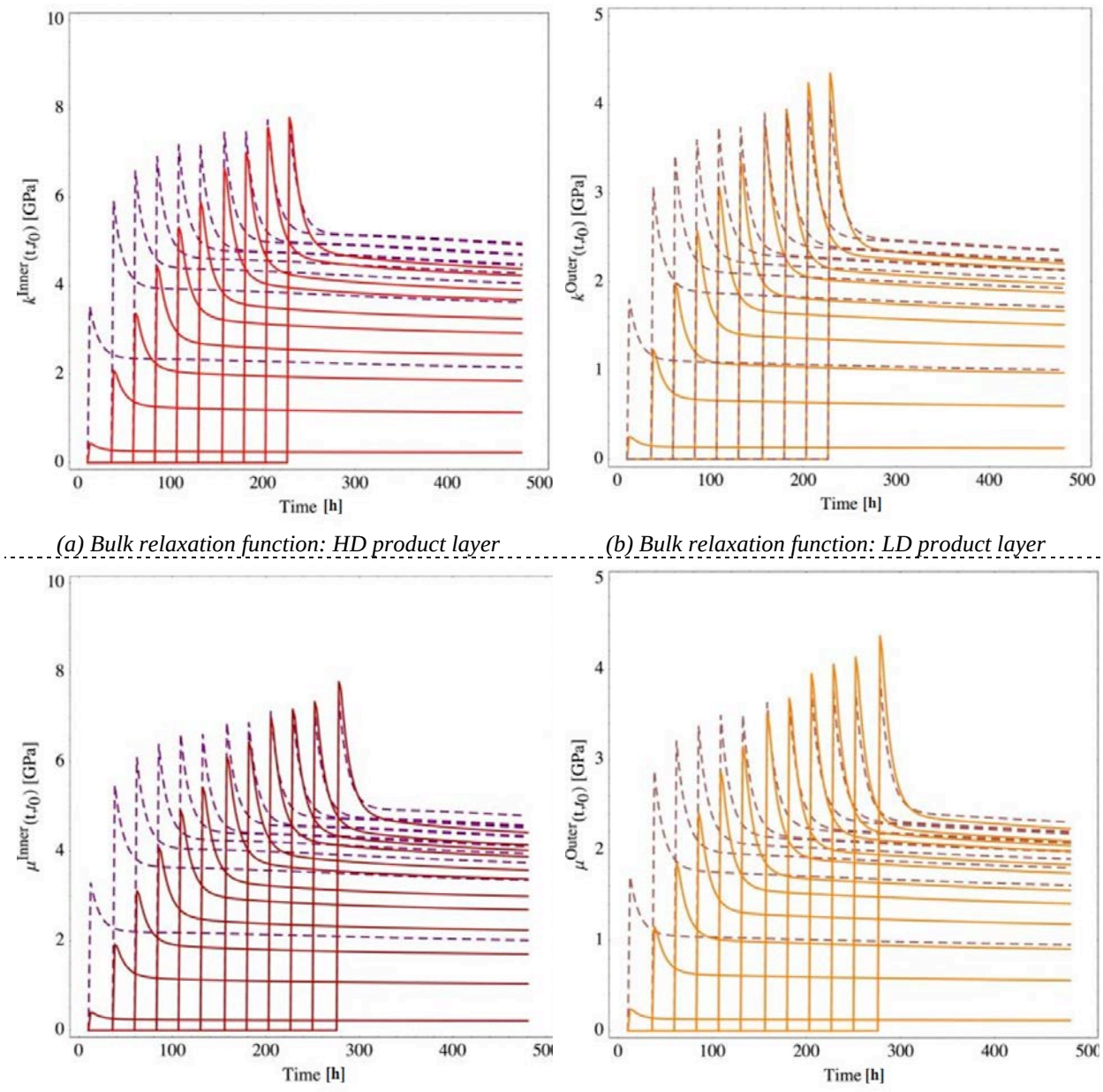

(a) Bulk relaxation function: HD product layer

(b) Bulk relaxation function: LD product layer

(c) Shear relaxation function: HD product layer

(d) Shear relaxation function: LD product layer

Figure 11 Inner and outer layers: estimated bulk (top) and shear (bottom) relaxation functions for different loading ages with (full lines) and without (dashed) space-filling

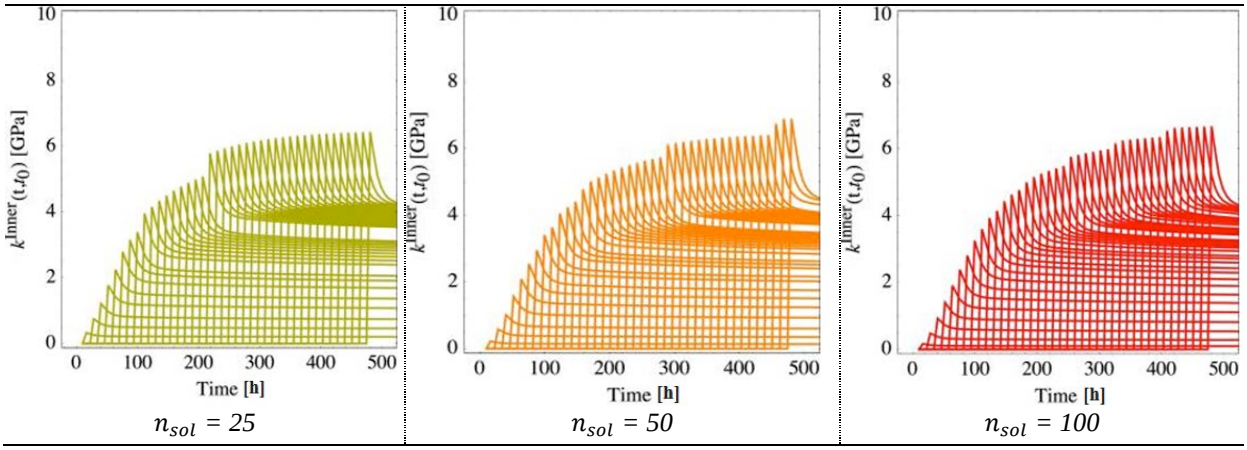

Figure 12 Effect of the discretization of the ageing function on the bulk relaxation function of the HD product layer

The estimated effective bulk and shear relaxation functions as well as the creep function of the cement paste are shown in Figure 13 and Figure 14, respectively. We adopted n_{sol} = *50*. The early behaviour in both cases are quite different, with the space-filling scenario, as expected from Fig. 2 and 4-5, creeping more at very early ages than the scenario without space-filling. Similarly to the C-S-H behaviour, after about 300 h the ageing character of the response vanishes for the case without space filling. A delayed effect is observed due to the space filling in the other scenario in which the ageing character vanishes after about 400 h.

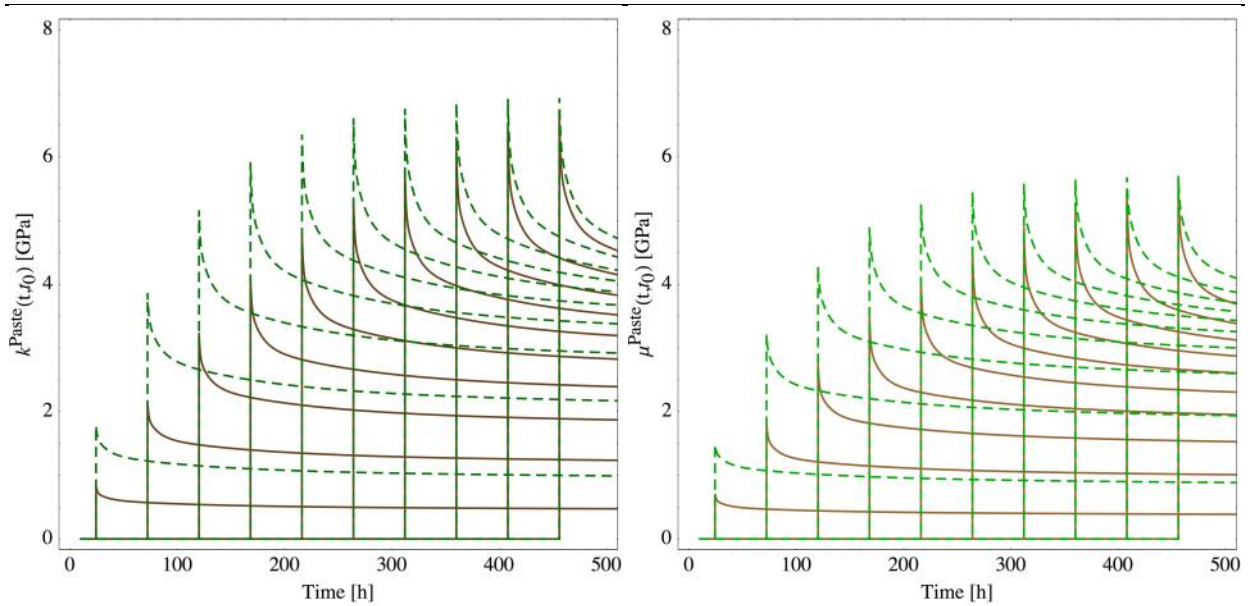

(a) Bulk relaxation function ***(b) Shear relaxation function***

Figure 13 Effective behaviour of the cement paste: bulk (left) and shear (right) relaxation functions for behaviours with (full brown lines) and without (green dashed lines) space filling

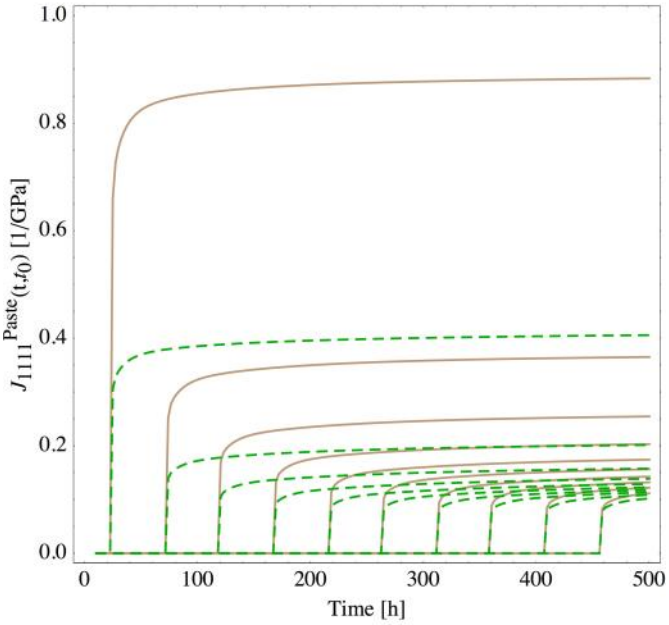

Figure 14 Effective behaviour of the cement paste: creep function with (full brown lines) and without (green dashed lines) space filling

6. MORTAR SCALE

At the mortar scale (Level 3), a 3-phase composite sphere is employed to represent the microstructure (Figure 1). The core corresponds to the sand particle. We adopt the volume fraction of sand f_{Sand} = 50%. The first coat is the ITZ and the second coat is the cement paste whose behaviour was obtained in the previous section. Note that, differently of the cement paste scale, the volume fractions of the three phases in the coated sphere morphology at the mortar scale remain the same; so no additional ageing from solidification processes occurs at this scale.

6.1 DEFINITIONS OF ITZ VOLUME AND COMPOSITION

The mechanical properties of the ITZ are reported to be inferior to those of the cement paste. We assume that the ITZ is composed of C-S-H LD and a part of the other hydration products, water, gypsum and empty pores from the cement paste. The part of the products and reactants going to the ITZ is discounted from the C-S-H LD coat. In this sense, the composition of the LD layer in Figure 8 changes as a function of the volume and composition of the ITZ. The aspects related to the definitions of these features are discussed in this section.

Experimental evidence shows that the matrix of the mortar and the hardened cement paste present different porosities [33]. We assume that this difference is due to the ITZ higher porosity compared to the cement paste. We adopted a supplementary porosity of the mortar matrix with respect to the cement paste of 10%, which is similar to the difference in porosity obtained by Heukamp [33]. Also, the ITZ is likely to contain more CH and AF-phases [57]. These aspects are considered in the

composition of the ITZ as shown in Figure 17. Compared to the LD layer solid phases, the ITZ here owns 5% more CH and AF-phases, following the results of Sun et al. [57] (average of CH content within the first 20 μm for w/c = 0.50); the C-S-H content was minored by 5% to compensate this addition.

To compute the volume of the ITZ according to the PSD $w(R_0)$ of sand, we adopt the approach developed in [58] resorting to the nearest neighbour surface distribution function $e_v(r)$. In a system of polydisperse non-correlated spheres, this function allows accounting for the likely interpenetration of the ITZs. Depending on the number of particles ρ with a given size, the volume of the ITZ V_{ITZ} can be estimated in terms of $e_v(r)$. For a given thickness of the ITZ e_{ITZ} , we have [58]:

$$V_{ITZ} = 1 - V_{agg} - e_v(e_{ITZ}) \tag{18}$$

where V_{agg} is the volume fraction of aggregates and [59,60]

$$e_v(r) = (1 - V_{agg}) \exp[-\pi\rho(a\, r + b\, r^2 + c\, r^3] \tag{19}$$

where:

$$\begin{aligned} a &= \frac{4\langle {R_0}^2 \rangle}{1 - V_{agg}} \\ b &= \frac{4\langle R_0 \rangle}{1 - V_{agg}} + \frac{12\, \mathcal{B}\langle {R_0}^2 \rangle}{\left(1 - V_{agg}\right)^2} \\ c &= \frac{4}{3\left(1 - V_{agg}\right)} + \frac{8\, \mathcal{B}\langle R_0 \rangle}{\left(1 - V_{agg}\right)^2} + \frac{16\, \mathcal{A}\, \mathcal{B}^2\langle {R_0}^2 \rangle}{3\left(1 - V_{agg}\right)^3} \end{aligned} \tag{20}$$

with $\langle f \rangle = \int_0^\infty w(R_0)\ \mathrm{f}(r, R_0)\, dR_0$ being the first momentum of a function f; $\mathcal{B} = 2\pi\rho\langle {R_0}^2 \rangle/3$ and $\mathcal{A}$ being a parameter equal to 0, 2 or 3 depending on the approximation chosen. [58] used $\mathcal{A}$= 0 in theirs simulations; the same value is adopted in the following.

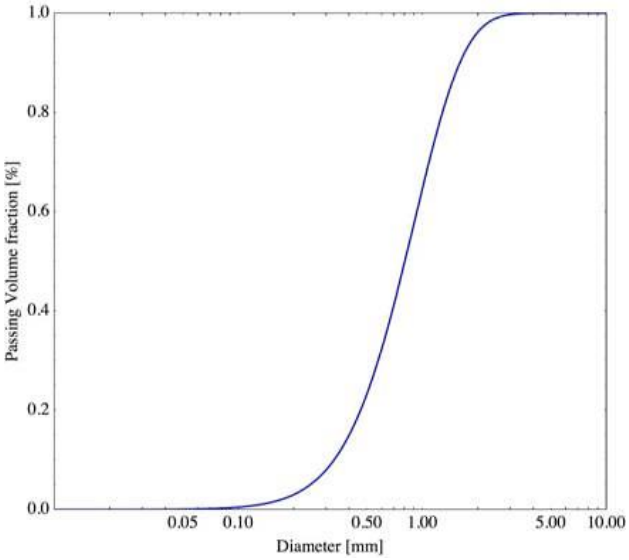

Figure 15 Passing volume fraction of sand used in the simulation (sand 0/4)

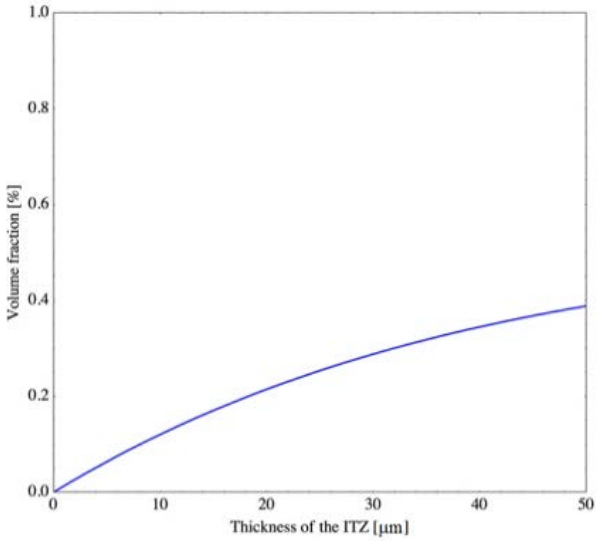

Figure 16 ITZ volume fraction according to the thickness of the ITZ (e_{ITZ})

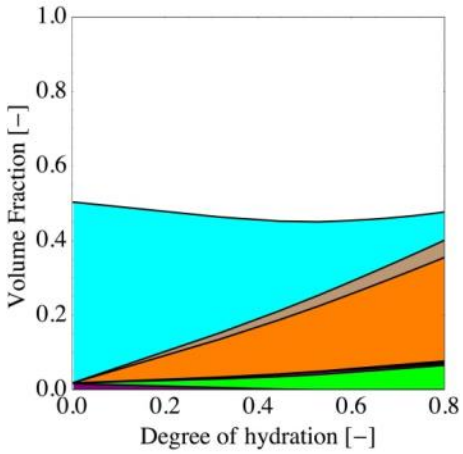

Figure 17 Composition of the ITZ for e_{ITZ}= *20 µm* (same legend as in Figure 7)

The passing volume fraction of the sand used in the simulations is shown in Figure 15. The volume fraction of the ITZ in the mortar using the formulation presented in Eqs. (18) – (20) is presented in Figure 16 for the same sand PSD. Of course, if e_{ITZ} tends towards infinity there is no more 'paste' but only ITZ + sand. As expected, the volume of the ITZ depends strongly on the thickness e_{ITZ} adopted. This, due to the assumptions regarding the composition of the ITZ, will specially reverberate in the estimation of ITZ porosity. In the following we adopt e_{ITZ}= *20 µm* (a value commonly reported in the literature [61,62]). It should be noted that for $e_{ITZ} = 20$ *µm* about half of matrix is composed of ITZ, which may be questionable in the case of a homogeneous ITZ (constant properties along ITZ thickness instead of a gradation of properties). It is also worthy to recall that small sand particle cannot contribute significantly to the so-called wall-effect. These aspects deserve to be more deeply studied. The resulting composition of the ITZ is shown in Figure 17.

6.2 EFFECTIVE PROPERTIES AT THE MORTAR SCALE

The properties of the ITZ layer are first determined. Figure 18 shows the estimated bulk and shear relaxation function of the ITZ with the composition presented in Figure 17. Compared to the LD layer in Figure 11, the behaviour is less stiff.

The estimated effective bulk and shear relaxation functions as well as the creep function of the mortar are shown in Figure 19 and Figure 20, respectively, for different loading ages. Only a slight ageing character is observed after 400 h for both scenarios with and without space filling.

As expected, cement paste (Figure 14) creeps more than mortar (Figure 20), even if the ITZ creep strains (not shown for conciseness) are more elevated than cement paste creep strains.

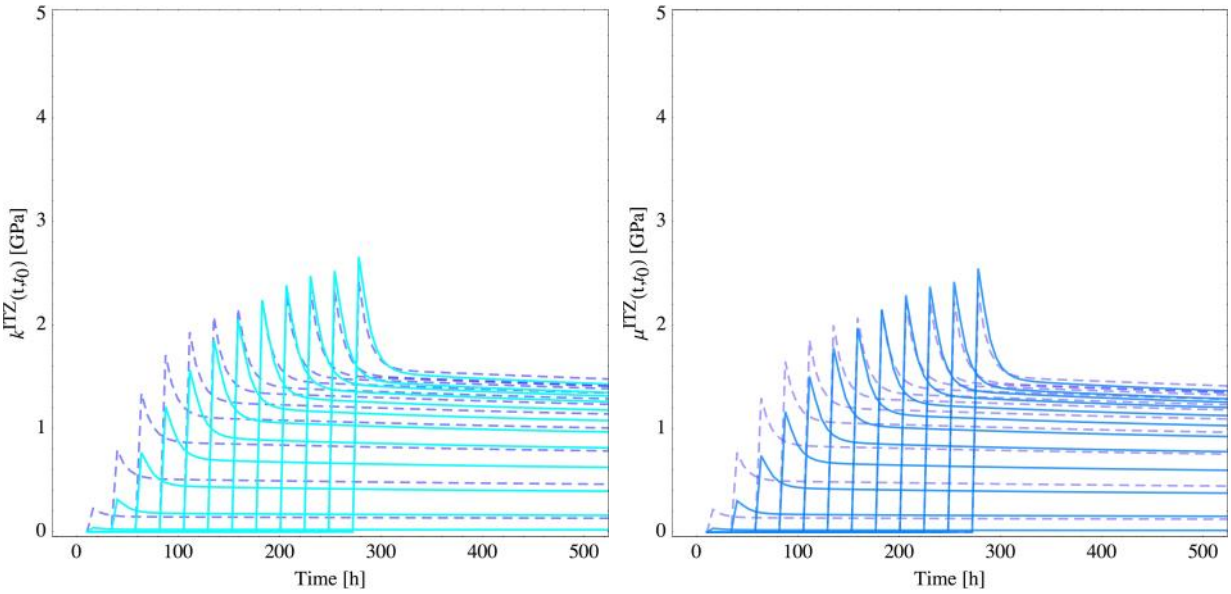

(a) Bulk relaxation function *(b) Shear relaxation function*

Figure 18 ITZ: estimated bulk (left) and shear (right) relaxation functions of behaviours with (full lines) and without (dashed lines) space-filling (to be compared with LD layer, see Figure 11)

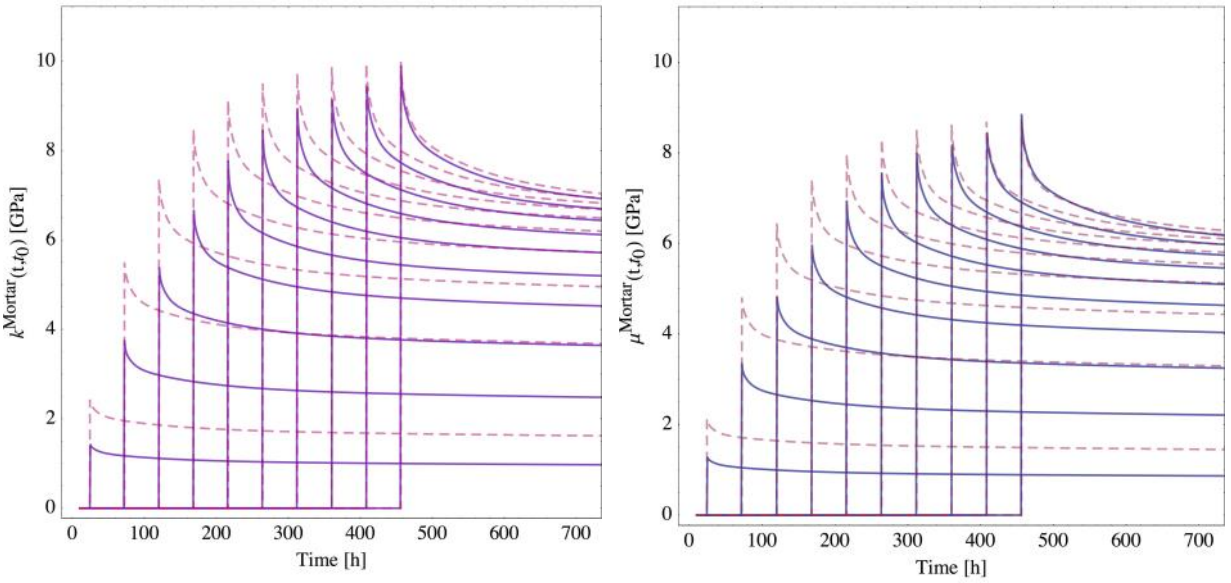

(a) Bulk relaxation function

(b) Shear relaxation function

Figure 19 Effective behaviour of mortar: bulk (left) and shear (right) relaxation functions for behaviours with (full blue lines) and without (pink dashed lines) space filling

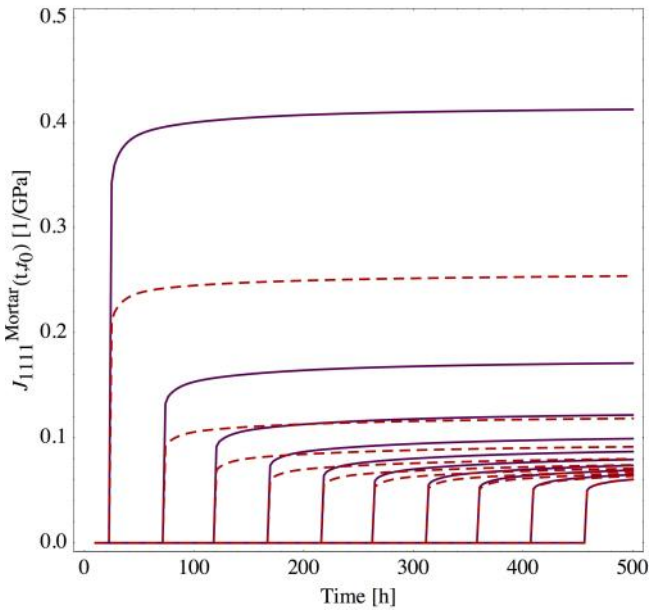

Figure 20 Effective behaviour of the mortar: creep function with (full purple lines) and without (red dashed lines) space filling

Figure 21 shows the effect of unloading on strains after a classical creep loading. Note that an important part of creep strains is not recovered on unloading due to the ageing character. Also, these residual strains are greater for later unloading. These aspects would deserve further investigations and confrontations against experimental data.

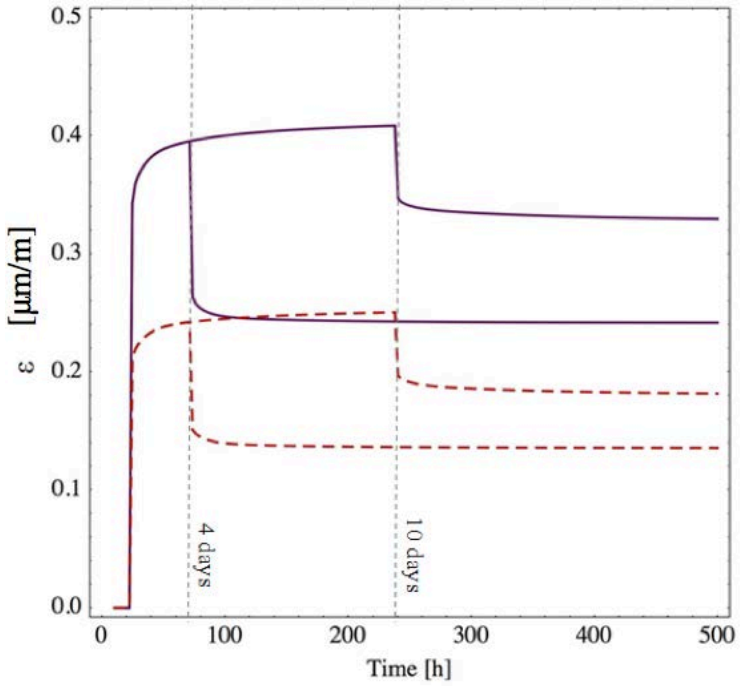

Figure 21 Unloading effects: Mortar creep strains (initial load = 1 MPa) with (full purple lines) and without (red dashed lines) space filling. Unloading at 4 and 10 days.

7. CONCRETE SCALE

At the concrete scale (Level 4), numerical homogenization is used to estimate the properties. Two phases are considered: the coarse aggregates with elastic behaviour and the mortar matrix with ageing viscoelastic behaviour obtained from the previous sections. Note that, since the specific surface of coarse aggregates is much smaller than that of the sand, the ITZ of the coarse aggregates are not considered. Bary et al. [63] showed, by means of numerical simulations, that the ITZ of coarse aggregate are indeed negligibly influential in a non-ageing viscoelastic context.

Two numerical samples with volume fraction of coarse aggregates f_{Gra} = 40% are studied: a) with spherical inclusions and (b) with convex polyhedral inclusions obtained from Voronoi decomposition [36]. The mesostructures tested are shown in Figure 22. These numerical samples are generated by randomly distributing the inclusions in a box. The procedure for constructing the mesostructures is detailed in [34] and [64]. The open-source python library Combs based on the Computer-Aided Design code Salome (www.salome-platform.org) is used to generate geometry and meshes of the mesostructures [34]. The GJK 3D algorithm has been recently implemented in Combs for fast convex particles distance computation (see e.g. http://www.dyn4j.org/2010/04/gjkdistance-closest-points).

For the local information assessment, the matrix is divided in 512 elements. Static uniform boundary conditions (SUBC) are adopted, which is reported to return more adequate results for composites in which the inclusions are stiffer than the matrix [17,65] than kinematic uniform

boundary conditions. The PSD of the inclusions in both meshes is shown in Figure 23. The isotropy of both mesostructures was successfully verified (not shown here for conciseness).

The simulations are performed with the finite elements code Cast3M (www.cast3m.fr), in which the ageing viscoelastic constitutive behaviour is implemented by means of the MFront code generator (http://tfel.sourceforge.net/) following an algorithm similar to the one of [66].

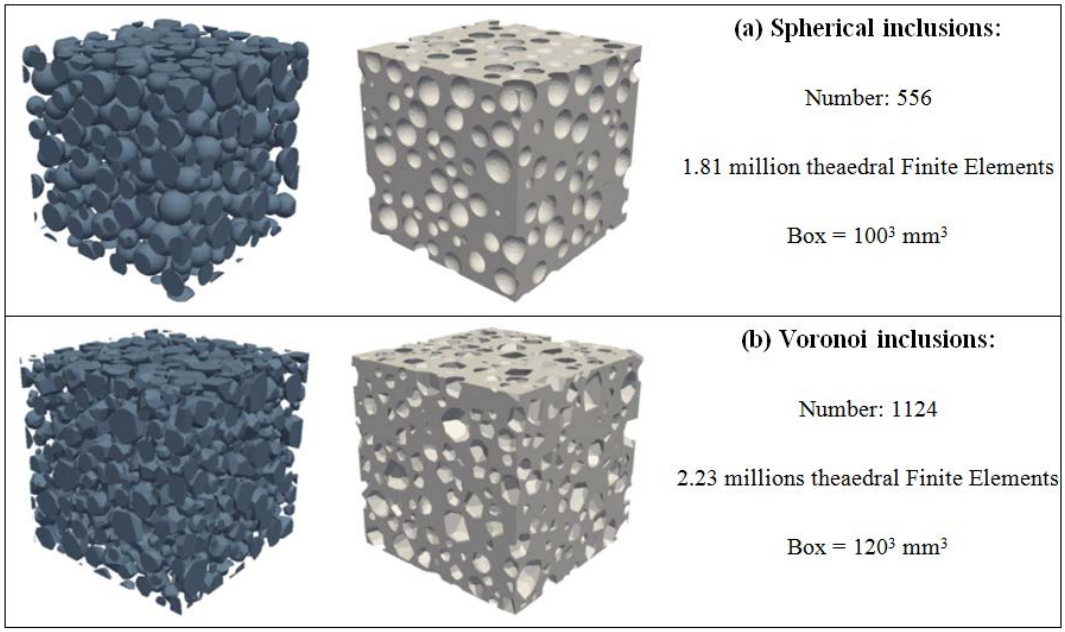

Figure 22 Mesostructures with matrix and spherical inclusions (up) and Voronoi inclusions (down) used in FEM simulations

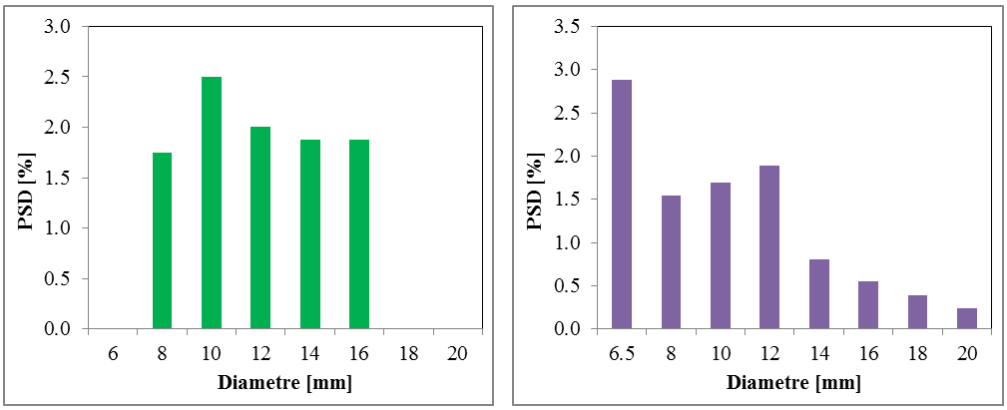

(a) Spherical inclusions *(b) Voronoi inclusions*

Figure 23 Particle size distribution of the inclusions in both meshes (a) Spherical and (b) Voronoi inclusions

7.1 EFFECTIVE PROPERTIES AT THE CONCRETE LEVEL

At the concrete scale, to ease the numerical implementation the behaviour of the mortar is fitted on the macroscopic one obtained by analytical homogenization by means of Prony series multiplied by an ageing function. Figure 24 shows an example of this fitting. Note that a surface (Figure 24 right) needs to be fitted since the relaxation functions depend on both time t and loading time t_0. Each simulation took about 3h for computing 30 time steps and effectuating the post processing on a computer with 16 cores, 2.0 GHz frequency and memory with 64Gb DDR 3 1600 MHz.

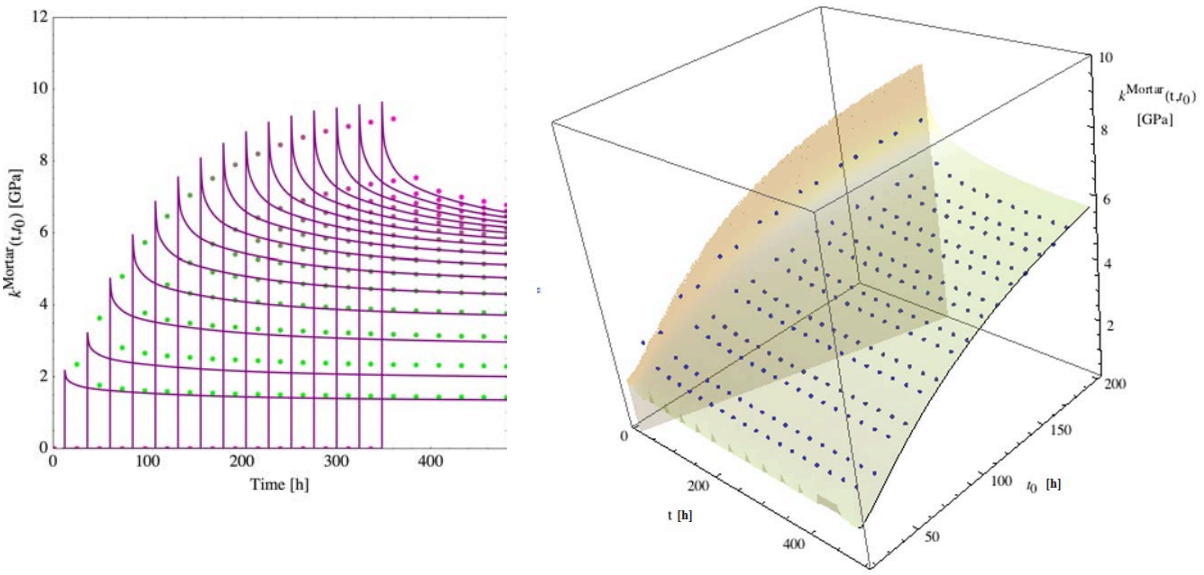

Figure 24 Fitting of the relaxation function of mortar: example of the bulk relaxation function for the no space-filling case. Left: The points are the estimations obtained by analytical homogenization. The full lines are the fitting. The same results are shown on the right picture: the points are the estimations obtained by analytical homogenization and the surface is the fitting.

The calculated effective bulk and shear relaxation functions as well as the creep function of the concrete are shown in Figure 25 and Figure 26, respectively. With the mortar behaviours computed in the last section, the ageing character is reproduced in the effective behaviour of concrete for both cases (with and without space filling).

The creep values obtained for both mortar behaviours are in agreement with some values found in the literature (e.g. [67]). The scenario with space filling creeps more at the very early age. Note that the values of the relaxation properties are slightly different for the mesostructure with spherical inclusions compared to the one with Voronoi inclusions for both scenarios. The difference is more accentuated in the creep function calculations. The higher the contrast is (here, the earlier the loading time), the bigger the difference is between both simulations.

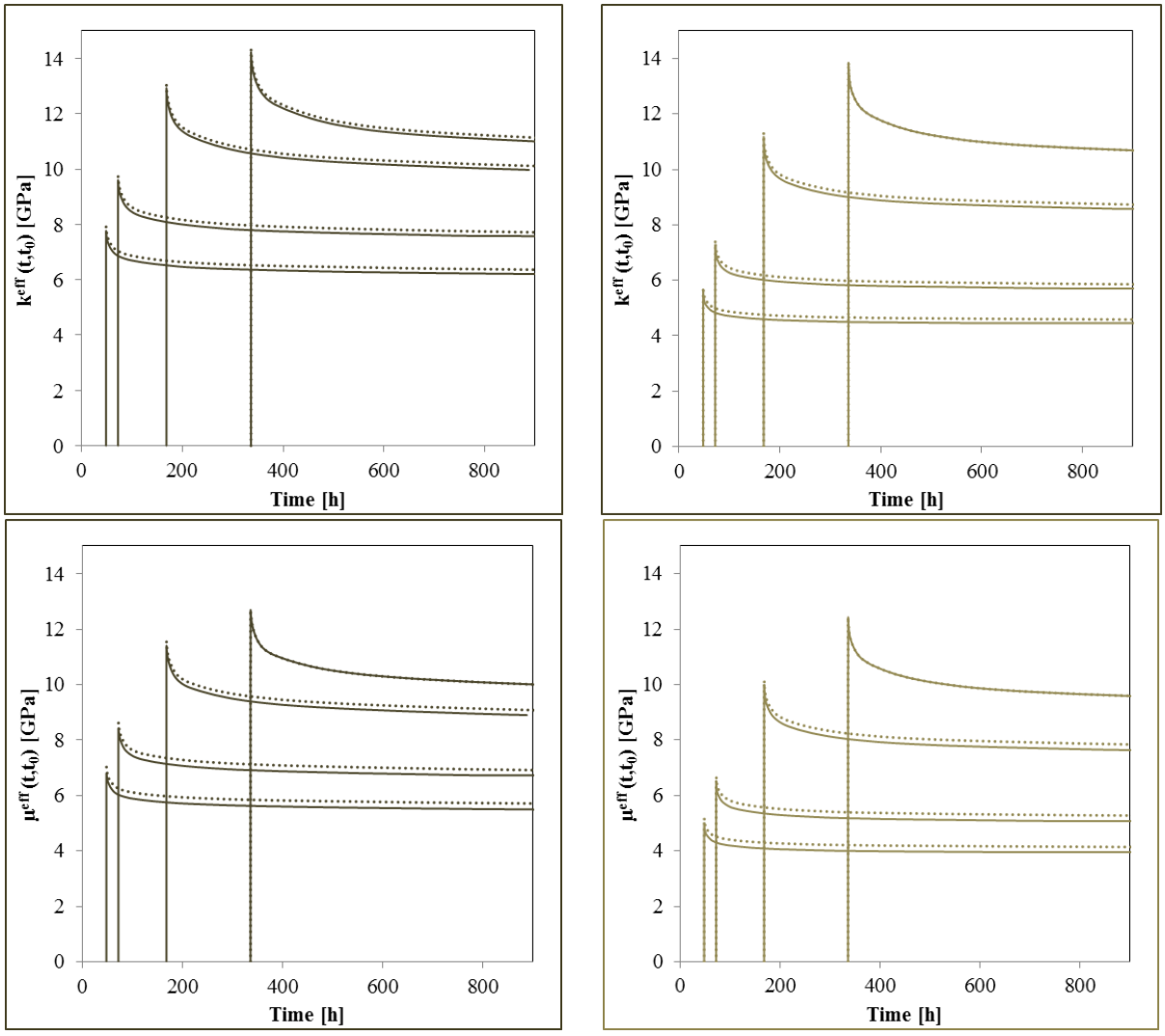

(a) without space-filling *(b) with space-filling*

Figure 25 Calculated bulk (up) and shear (down) relaxation functions of concrete obtained by simulations for different loading ages: comparison between the mesostructures with spherical (full lines) and Voronoi (dotted lines) inclusions for scenarios with (right) and without (left) space-filling

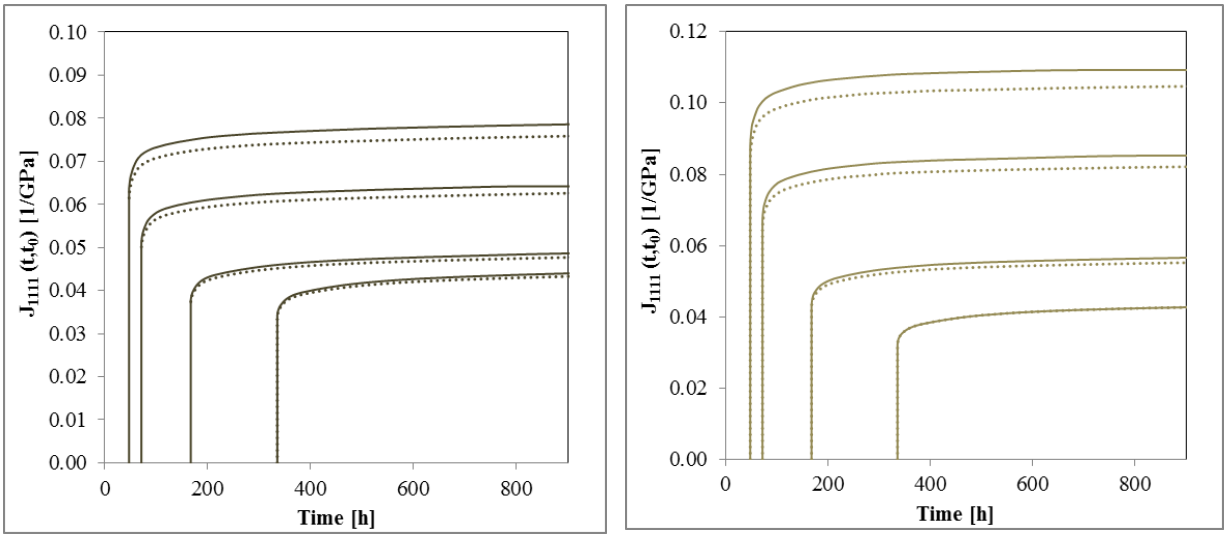

(a) without space-filling *(b) with space-filling*

Figure 26 Overall uniaxial creep function of concrete obtained by simulations for different loading ages: comparison between the mesostructures with spherical (full lines) and Voronoi (dotted lines) inclusions for scenarios with (right) and without (left) space-filling

7.2 LOCAL INFORMATION

As mentioned in the introduction, numerical homogenization allows assessing local information such as the average stress and strains within each inclusion or matrix subvolumes, which cannot be obtained analytically. In the following, a compressive loading of 25.6 MPa is applied on one of the faces of the numerical sample, and the local analysis is performed in terms of average strain in the direction of the loading.

Regarding the inclusions, Figure 27 shows the distributions of the average uniaxial strain according to the mortar behaviour and the type of inclusions, for a loading time equal to 2 days and for different times. Similar distributions of the strain are observed for spherical and polyhedral inclusions. A small impact of the mortar behaviour (with or without space filling) is observed, in both cases the distributions do not evolve significantly as a function of time. Because some inclusions are in contact with the loaded surfaces, some outliers are observed among the inclusions. This aspect can be bypassed by taking as a sample a fraction of the box in which the edges are excluded in the post processing.

Regarding the matrix, the distributions of strains tend to get broader with the time (Figure 28). The shape of the inclusions seems to affect them poorly.

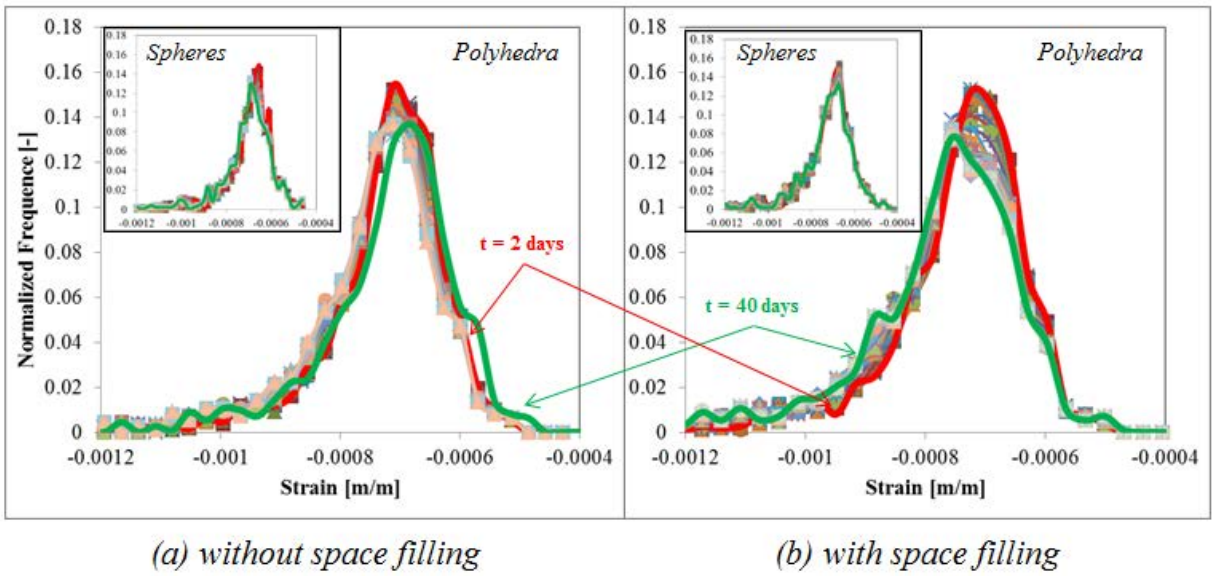

Figure 27 Distribution of the average uniaxial strain within the inclusions, t_0 = *2 days*

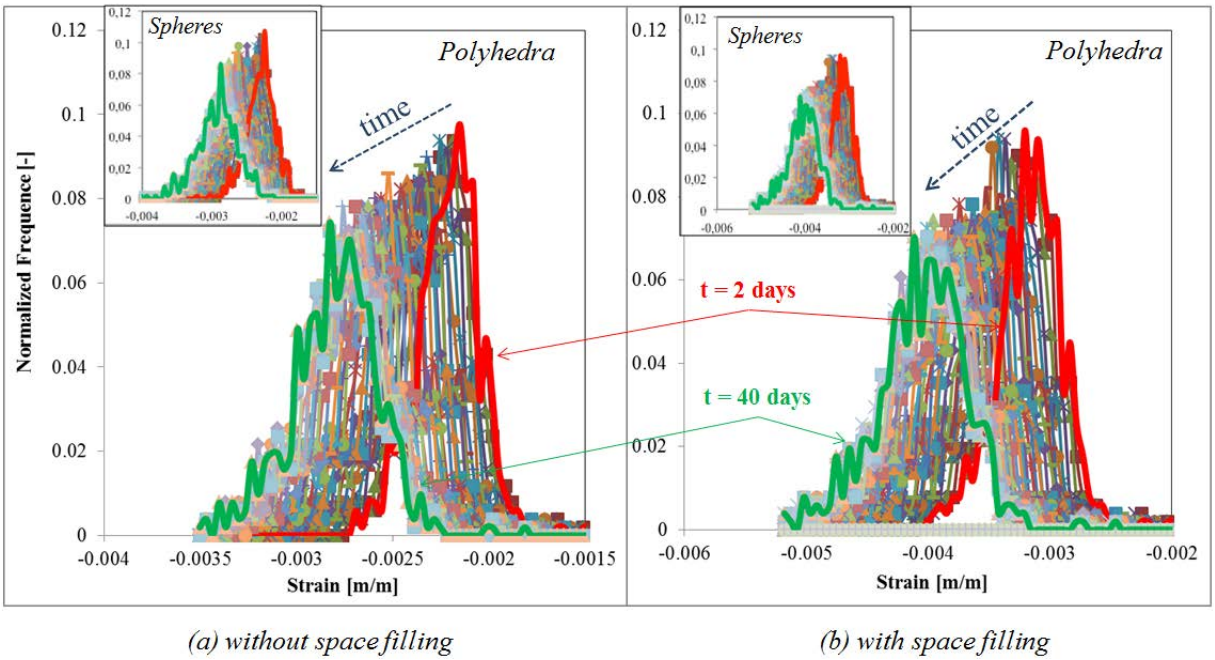

Figure 28 Distribution of the uniaxial strain for the matrix, t_0 = *2 days*

Figure 29 shows the maps of strains in the sample with polyhedral inclusions, in the direction of the loading, at two times and for t_0 = 2 days. The presence of zones with higher magnitude of strains is evident for the case with space-filling (covering the full colour range in Figure 29) .

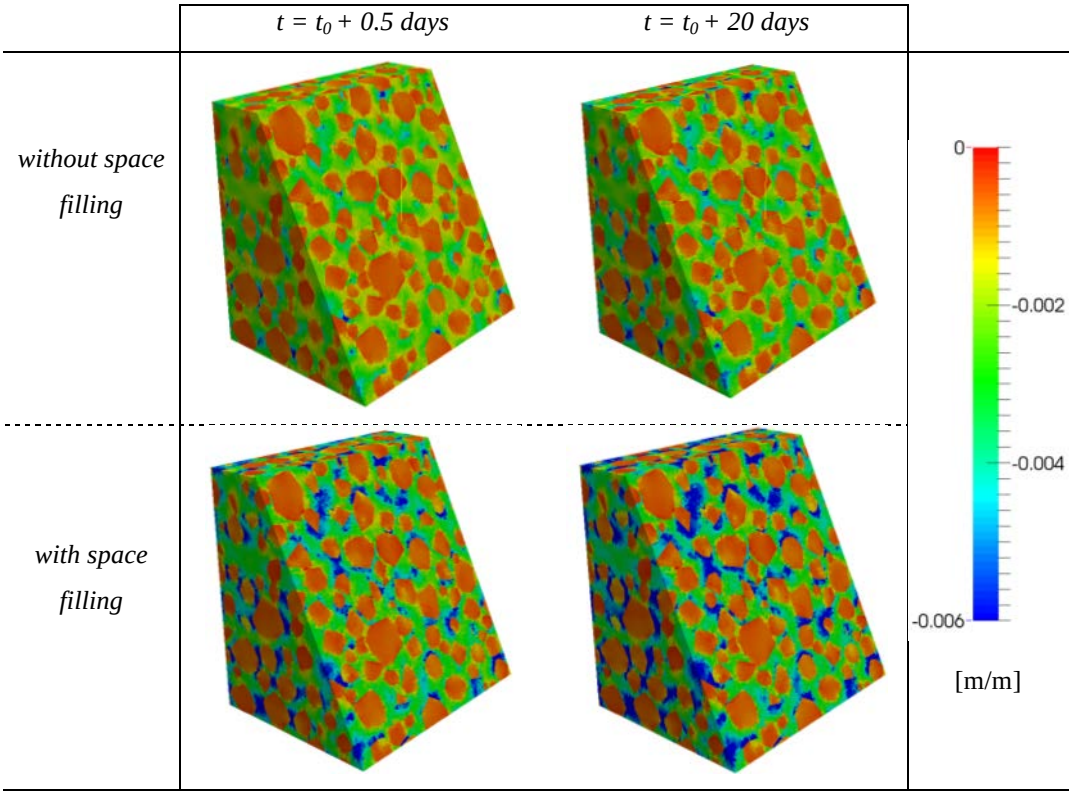

Figure 29 Strains (in the direction of the loading) within aggregates and mortar matrix in the sample with polyhedral inclusions at different ages for t_0 = 2 days

7.3 COMPARISON WITH EXPERIMENTAL DATA

The estimations of the creep of concrete according to the combined numerical and analytical strategy presented in this paper is compared to the experimental results obtained by Craeye et al. [68] for a concrete composed by the cement with the composition shown in Table 1 and a formulation in terms of w/c, sand and aggregates as the one used in the simulations. The comparison of the results of basic creep (with the elastic part discounted) is shown in Figure 30. The mortar behaviour with space filling returns results closer to the experimental results. In this case, a slightly better agreement is observed for spherical inclusions. Further comparisons are needed to benchmark the effects of the space filling on the behaviour of concrete. In particular, it would be appreciable to validate the model estimations against experimental data of cement pastes and mortars, which would also justify the developments regarding the ITZ effects.

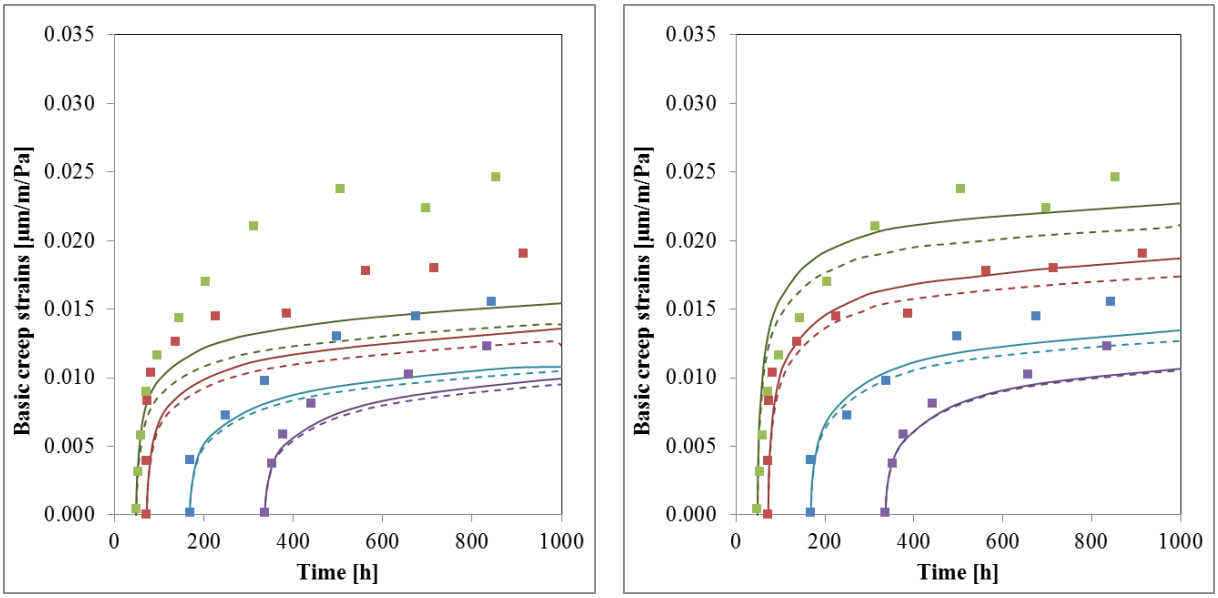

(a) without space-filling *(b) with space-filling*

Figure 30 Basic creep of concrete obtained experimentally (symbols, [68]) and by the modelling for different loading ages: comparison between the mesostructures with spherical (full lines) and Voronoi (dashed lines) inclusions for scenarios with (right) and without (left) space-filling

8. CONCLUSIONS AND PERSPECTIVES

In this paper, a strategy combining analytical and numerical homogenization tools was employed to investigate the ageing viscoelastic behaviour of cement-based materials at early-age. Analytical schemes were used to estimate the properties at the level of hydration products, cement paste and mortar. Numerical homogenization was used to study the concrete scale. This combined approach allowed investigating different propositions of mechanisms leading to an ageing behaviour. Simulations taking into account the space-filling process as leading to an intrinsically ageing behaviour of C-S-H were compared to simulations in which this effect was not considered. The obtained results allow concluding:

- The estimations of the creep response are in agreement with the usual values obtained experimentally for similar concretes. At all levels (cement paste, mortar and concrete) the material creeps more at the very early-age when the behaviour accounting for the space-filling is adopted.
- The behaviour with space filling returned results closer to the experimental values of creep measured for a concrete with the composition studied. Note however, that the dependency of the estimations on the model parameters used, some of them being inaccurately known, does not allow concluding that the estimations with space filling are indeed more adequate. Further investigations are needed to benchmark the need of accounting for the space-filling (or other mechanisms contributing to the ageing character of the material) in the estimation of

viscoelastic properties of cement-based materials at early age, ideally with creep or relaxation tests at the cement paste, mortar and concrete scales.

- The inclusions shape affects not very strongly the overall behaviour. The earlier the loading time the higher the difference between the response of polyhedral and spherical inclusions. The local information obtained by numerical homogenization at the concrete level shows a similar dispersion of the strains for both inclusions shapes.

As limitations and perspectives, we highlight:

- The upscaling approach presented here is valid only for periods after the percolation of the microstructure. Strategies to account for the existence of a percolation threshold at the cement paste level are to be developed.
- The influence of the ITZ on the ageing linear viscoelastic behaviour deserves further investigations. Mortar behaviours estimated with different ITZ thicknesses and compositions can be performed. Additionally, an adaptation of the GSC so that a fixed ITZ thickness, independent of the size of the particle, is set is another aspect to be considered.
- The mortar level can be itself studied by means of numerical homogenization too. For example, a two-coated microstructure (as in [17]) could be used to represent the mesostructure of mortar. But inherent difficulties regarding the representation of the ITZ with its interpenetrations, as well as the small thickness of ITZ which demands a much finer meshing, makes this extension not trivial.
- Further studies accounting for the effect of the volume fraction of the inclusions and phase contrast on the ageing linear viscoelastic behaviour can be envisaged.

Acknowledgements

This present work has been performed as part of the project on disposal of LILW-SL that is carried out by ONDRAF/NIRAS, the Belgian Agency for Radioactive Waste and enriched Fissile Materials.

9. REFERENCES

[1] S. Yip, M.P. Short, Multiscale materials modelling at the mesoscale, Nat. Mater. 12 (2013) 774–777. doi:10.1038/nmat3746.

[2] P. Acker, Swelling, shrinkage and creep: a mechanical approach to cement hydration, Mater. Struct. 37 (2004) 237–243. doi:10.1007/BF02480632.

[3] O. Bernard, F.-J. Ulm, E. Lemarchand, A multiscale micromechanics-hydration model for the early-age elastic properties of cement-based materials, Cem. Concr. Res. 33 (2003) 1293–1309.

[4] G. Constantinides, F.-J. Ulm, The effect of two types of C-S-H on the elasticity of cement-based materials: Results from nanoindentation and micromechanical modeling, Cem. Concr. Res. 34 (2004) 67–80. doi:10.1016/S0008-8846(03)00230-8.

[5] Z. Hashin, P.J.M. Monteiro, An inverse method to determine the elastic properties of the interphase between the aggregate and the cement paste, Cem. Concr. Res. 32 (2002) 1291–1300.

[6] J. Sanahuja, L. Dormieux, G. Chanvillard, Modelling elasticity of a hydrating cement paste, Cem. Concr. Res. 37 (2007) 1427–1439.

[7] F.-J. Ulm, G. Constantinides, F.H. Heukamp, Is concrete a poromechanics materials?—A multiscale investigation of poroelastic properties, Mater. Struct. 37 (2004) 43–58. doi:10.1007/BF02481626.

[8] M.-Q. Thai, B. Bary, Q.-C. He, A homogenization-enriched viscodamage model for cement-based material creep, Eng. Fract. Mech. 126 (2014) 54–72. doi:10.1016/j.engfracmech.2014.04.021.

[9] G.N. Maslov, Thermal Stress States in Concrete Masses, with Account of Concrete Creep, Izv. NIIG Gosenergoizdat. 28 (1940) 175–188.

[10] J. Lubliner, J.L. Sackman, On ageing viscoelastic materials, J. Mech. Phys. Solids. 14 (1966) 25–32. doi:10.1016/0022-5096(66)90017-2.

[11] Z.P. Bazant, A.B. Hauggaard, S. Baweja, F.-J. Ulm, Microprestress-solidification theory for concrete creep. I: Aging and drying effects, J. Eng. Mech. 123 (1997) 1188–1194.

[12] Z.P. Bazant, C. Huet, Thermodynamic functions for ageing viscoelasticity - integral form without internal variables.pdf, Int. J. Solids Struct. (1999).

[13] S. Scheiner, C. Hellmich, Continuum microviscoelasticity model for aging basic creep of early-age concrete, J. Eng. Mech. 135 (2009) 307–323.

[14] J. Sanahuja, Efficient Homogenization of Ageing Creep of Random Media: Application to Solidifying Cementitious Materials, in: American Society of Civil Engineers, 2013: pp. 201–210. doi:10.1061/9780784413111.023.

[15] J. Sanahuja, Effective behaviour of ageing linear viscoelastic composites: Homogenization approach, Int. J. Solids Struct. 50 (2013) 2846–2856. doi:10.1016/j.ijsolstr.2013.04.023.

[16] J. Salençon, Viscoélasticité pour le calcul des structures, Editions Ecole Polytechnique, 2009.

[17] T. Honorio, B. Bary, J. Sanahuja, F. Benboudjema, Effective properties of n-coated composite spheres assemblage in an ageing viscoelastic framework, (under review).

[18] F. Lavergne, K. Sab, J. Sanahuja, M. Bornert, C. Toulemonde, Investigation of the effect of aggregates' morphology on concrete creep properties by numerical simulations, Cem. Concr. Res. 71 (2015) 14–28. doi:10.1016/j.cemconres.2015.01.003.

[19] H. Sadouki, F.H. Wittmann, On the analysis of the failure process in composite materials by numerical simulation, Mater. Sci. Eng. A. 104 (1988) 9–20. doi:10.1016/0025-5416(88)90401-6.

[20] J. Sanahuja, C. Toulemonde, Numerical homogenization of concrete microstructures without explicit meshes, Cem. Concr. Res. 41 (2011) 1320–1329. doi:10.1016/j.cemconres.2011.03.023.

[21] H. Schorn, U. Rode, Numerical simulation of crack propagation from microcracking to fracture, Cem. Concr. Compos. 13 (1991) 87–94. doi:10.1016/0958-9465(91)90003-Z.

[22] Z.M. Wang, A.K.H. Kwan, H.C. Chan, Mesoscopic study of concrete I: generation of random aggregate structure and finite element mesh, Comput. Struct. 70 (1999) 533–544. doi:10.1016/S0045-7949(98)00177-1.

[23] P. Wriggers, S.O. Moftah, Mesoscale models for concrete: Homogenisation and damage behaviour, Finite Elem. Anal. Des. 42 (2006) 623–636. doi:10.1016/j.finel.2005.11.008.

[24] S. Bishnoi, K.L. Scrivener, μic: A new platform for modelling the hydration of cements, Cem. Concr. Res. 39 (2009) 266–274. doi:10.1016/j.cemconres.2008.12.002.

[25] Q.H. Do, Modelling Properties of Cement Paste from Microstructure: Porosity, Mechanical Properties, Creep and Shrinkage, EPFL, 2013. http://infoscience.epfl.ch/record/187639/files/EPFL_TH5881.pdf (accessed June 5, 2015).

[26] D.P. Bentz, CEMHYD3D: A Three-Dimensional Cement Hydration and Microstructure Development Modeling Package. Version 3.0. NISTIR 7232. National Institute of Standards and Technology Interagency Report, Technology Administration, U.S. Department of Commerce, NISTIR 7232, (2005).

[27] K. Van Breugel, Simulation of Hydration and Formation of Structure in Hardening Cement-Based Materials—HYMOSTRUC, (1997).

[28] M. Briffaut, F. Benboudjema, La Borderie, Christian, J.-M. Torrenti, Creep Consideration Effect on Meso-Scale Modeling of Concrete Hydration Process and Consequences on the Mechanical Behavior, J. Eng. Mech. 139 (2013) 1808–1817. doi:10.1061/(ASCE)EM.1943-7889.0000607.

[29] T. Honorio, B. Bary, F. Benboudjema, Estimation of Elastic Properties of Cement based Materials at Early Age based on a Combined Numerical and Analytical Multiscale Micromechanics Approach, in: RILEM Int. Symp. Concr. Model., Beijing, China, 2014.

[30] T. Honorio, B. Bary, F. Benboudjema, Multiscale estimation of the viscoelastic properties of cementitious materials at early age: a combined analytical and numerical approach, in: Mech. Physcis Shrinkage Creep Durab. Concr. CONCREEP 10, Wien, 2015. doi:0.1061/9780784479346.126.

[31] B. Bary, S. Béjaoui, Assessment of diffusive and mechanical properties of hardened cement pastes using a multi-coated sphere assemblage model, Cem. Concr. Res. 36 (2006) 245–258. doi:10.1016/j.cemconres.2005.07.007.

[32] E. Stora, B. Bary, Q.-C. He, E. Deville, P. Montarnal, Modelling and simulations of the chemo–mechanical behaviour of leached cement-based materials: Leaching process and induced loss of stiffness, Cem. Concr. Res. 39 (2009) 763–772. doi:10.1016/j.cemconres.2009.05.010.

[33] F.H. Heukamp, Chemomechanics of calcium leaching of cement-based materials at different scales : the role of CH-dissolution and C-S-H degradation on strength and durability performance of materials and structures, Thesis, Massachusetts Institute of Technology, 2003. http://dspace.mit.edu/handle/1721.1/29282 (accessed June 5, 2015).

[34] C. Bourcier, W. Dridi, L. Chomat, E. Laucoin, B. Bary, E. Adam, Combs: open source python library for RVE generation. Application to microscale diffusion simulations in cementitious materials, in: D. Caruge, C. Calvin, C.M. Diop, F. Malvagi, J.-C. Trama (Eds.), EDP Sciences, 2014: p. 02107. doi:10.1051/snamc/201402107.

[35] T. de Larrard, B. Bary, E. Adam, F. Kloss, Influence of aggregate shapes on drying and carbonation phenomena in 3D concrete numerical samples, Comput. Mater. Sci. 72 (2013) 1–14. doi:10.1016/j.commatsci.2013.01.039.

[36] B. Bary, L. Gélébart, E. Adam, C. Bourcier, Numerical analysis of linear viscoelastic 3D concrete specimens, in: Comput. Model. Concr. Struct., CRC Press, 2014: pp. 373–381. http://www.crcnetbase.com/doi/abs/10.1201/b16645-42 (accessed February 5, 2015).

[37] V. Volterra, Theory of functionals and of integral and integro-differential equations, CERN Doc. Serv. (1959). http://cds.cern.ch/record/268343 (accessed November 19, 2014).

[38] T. Mori, K. Tanaka, Average stress in matrix and average elastic energy of materials with misfitting inclusions, Acta Metall. 21 (1973) 571–574. doi:10.1016/0001-6160(73)90064-3.

[39] E. Herve, A. Zaoui, n-Layered inclusion-based micromechanical modelling, Int. J. Eng. Sci. 31 (1993) 1–10. doi:10.1016/0020-7225(93)90059-4.

[40] I. Carol, Z. Bažant, Viscoelasticity with Aging Caused by Solidification of Nonaging Constituent, J. Eng. Mech. 119 (1993) 2252–2269. doi:10.1061/(ASCE)0733-9399(1993)119:11(2252).

[41] P. Rossi, J.-L. Tailhan, F. Le Maou, L. Gaillet, E. Martin, Basic creep behavior of concretes investigation of the physical mechanisms by using acoustic emission, Cem. Concr. Res. 42 (2012) 61–73.

[42] J.J. Thomas, H.M. Jennings, A colloidal interpretation of chemical aging of the C-S-H gel and its effects on the properties of cement paste, Cem. Concr. Res. 36 (2006) 30–38. doi:10.1016/j.cemconres.2004.10.022.

[43] M. Vandamme, F.-J. Ulm, Nanogranular origin of concrete creep, PNAS. (2009).

[44] J. Sanahuja, L. Dormieux, Creep of a C-S-H gel: a micromechanical approach, An. Acad. Bras. Ciênc. 82 (2010) 25–41. doi:10.1590/S0001-37652010000100004.

[45] V. Smilauer, Z.P. Bazant, Identification of viscoelastic CSH behavior in mature cement paste by FFT-based homogenization method, Cem. Concr. Res. 40 (2010) 197–207.

[46] M. Vandamme, F.-J. Ulm, Nanoindentation investigation of creep properties of calcium silicate hydrates, Cem. Concr. Res. 52 (2013) 38–52. doi:10.1016/j.cemconres.2013.05.006.

[47] C.G. Hoover, F.-J. Ulm, Experimental chemo-mechanics of early-age fracture properties of cement paste, Cem. Concr. Res. 75 (2015) 42–52. doi:10.1016/j.cemconres.2015.04.004.

[48] S. Bishnoi, K. Scrivener, Studying nucleation and growth kinetics of alite hydration using μic, Cem. Concr. Res. 39 (2009) 849–860.

[49] T. Honorio, B. Bary, F. Benboudjema, S. Poyet, Modeling hydration kinetics based on boundary nucleation and space-filling growth in a fixed confined zone, Cem. Concr. Res. 83 (2016) 31–44. doi:10.1016/j.cemconres.2016.01.012.

[50] J.W. Bullard, H.M. Jennings, R.A. Livingston, A. Nonat, G.W. Scherer, J.S. Schweitzer, K.L. Scrivener, J.J. Thomas, Mechanisms of cement hydration, Cem. Concr. Res. 41 (2011) 1208–1223.

[51] Z.P. Bazant, Viscoelasticity of Solidifying Porous Material°Concrete, J. Eng. Mech. Div. 103 (1977) 1049–1067.

[52] K. Velez, S. Maximilien, D. Damidot, G. Fantozzi, F. Sorrentino, Determination by nanoindentation of elastic modulus and hardness of pure constituents of Portland cement clinker, Cem. Concr. Res. 31 (2001) 555–561.

[53] P.J.M. Monteiro, C.T. Chang, The elastic moduli of calcium hydroxide, Cem. Concr. Res. 25 (1995) 1605–1609. doi:10.1016/0008-8846(95)00154-9.

[54] S. Kamali, Comportement et simulation des matériaux cimentaires en environnement agressifs : Lixiviation et température, 2003. http://www.theses.fr/2003DENS0004.

[55] C.-J. Haecker, E.J. Garboczi, J.W. Bullard, R.B. Bohn, Z. Sun, S.P. Shah, T. Voigt, Modeling the linear elastic properties of Portland cement paste, Cem. Concr. Res. 35 (2005) 1948–1960. doi:10.1016/j.cemconres.2005.05.001.

[56] E. Stora, Multi-scale modelling and simulations of the chemo-mechanical behavior of degraded cement-based materials, Université Paris-Est, 2007.

[57] Z. Sun, E.J. Garboczi, S.P. Shah, Modeling the elastic properties of concrete composites: Experiment, differential effective medium theory, and numerical simulation, Cem. Concr. Compos. 29 (2007) 22–38. doi:10.1016/j.cemconcomp.2006.07.020.

[58] E.J. Garboczi, D.P. Bentz, Analytical formulas for interfacial transition zone properties, Adv. Cem. Based Mater. 6 (1997) 99–108. doi:10.1016/S1065-7355(97)90016-X.

[59] B. Lu, S. Torquato, Nearest-surface distribution functions for polydispersed particle systems, Phys. Rev. A. 45 (1992) 5530–5544. doi:10.1103/PhysRevA.45.5530.

[60] S. Torquato, Random Heterogeneous Materials: Microstructure and Macroscopic Properties, Springer Science & Business Media, 2002.

[61] M.K. Head, N.R. Buenfeld, Measurement of aggregate interfacial porosity in complex, multi-phase aggregate concrete: Binary mask production using backscattered electron, and energy dispersive X-ray images, Cem. Concr. Res. 36 (2006) 337–345. doi:10.1016/j.cemconres.2005.09.007.

[62] K.L. Scrivener, A.K. Crumbie, P. Laugesen, The Interfacial Transition Zone (ITZ) Between Cement Paste and Aggregate in Concrete, Interface Sci. 12 (2004) 411–421. doi:10.1023/B:INTS.0000042339.92990.4c.

[63] B. Bary, C. Bourcier, T. Helfer, Numerical analysis of concrete creep on mesoscopic 3D specimens, in: Wien, 2015.

[64] B. Bary, M.B. Haha, E. Adam, P. Montarnal, Numerical and analytical effective elastic properties of degraded cement pastes, Cem. Concr. Res. 39 (2009) 902–912. doi:10.1016/j.cemconres.2009.06.012.

[65] S. Pecullan, L.V. Gibiansky, S. Torquato, Scale effects on the elastic behavior of periodic andhierarchical two-dimensional composites, J. Mech. Phys. Solids. 47 (1999) 1509–1542. doi:10.1016/S0022-5096(98)00111-2.

[66] Z.P. Bažant, Numerical determination of long-range stress history from strain history in concrete, Matér. Constr. 5 (1972) 135–141. doi:10.1007/BF02539255.

[67] P. Laplante, Propriétés mécaniques des bétons durcissants: analyse comparée des bétons classiques et à très hautes performances, Ministère de l'equipement, des transports et du tourisme, Laboratoire central des ponts et chaussées, Paris, France, 1993.

[68] B. Craeye, G. De Schutter, H. Van Humbeeck, A. Van Cotthem, Early age behaviour of concrete supercontainers for radioactive waste disposal, Nucl. Eng. Des. 239 (2009) 23–35. doi:10.1016/j.nucengdes.2008.10.006.